Materials Meets Concepts in Molecule-Based Electronics

Frank Ortmann, K. Sebastian Radke, Alrun Günther, Daniel Kasemann, Karl Leo, and Gianaurelio Cuniberti*

In this contribution, molecular materials are highlighted as an important topic in the diverse field of condensed matter physics, with focus on their particular electronic and transport properties. A better understanding of their performance in various applications and devices demands for an extension of basic theoretical approaches to describe charge transport in molecular materials, including the accurate description of electron–phonon coupling. Starting with the simplest case of a molecular junction and moving on to larger aggregates of bulk organic semiconductors, charge-transport regimes from ballistic motion to incoherent hopping, which are frequently encountered in molecular systems under respective conditions, are discussed. Transport features of specific materials are described through ab initio material parameters whose determination is addressed.

1. Introduction

1.1. Molecular Materials in Current Applications

Molecular semiconductors differ from traditional semiconducting materials (such as Ge, Si, GaAs, etc.) in many regards including their mechanical, electrical, and optical properties, which is a direct consequence of their construction principles. While in traditional semiconductors, the basic building blocks are atoms that are strongly linked together by covalent or ionic bonds, organic semiconductors are based on molecular constituents, which are held together by much weaker van der Waals interaction.[1]

This has some advantages, as the molecules usually stay intact upon condensation[2] and molecular properties in gas phase and condensed phase are closely related, which allows one to adjust these properties already at the molecular-synthesis level. For instance, molecular properties can be exploited for optoelectronic devices in which these materials are very successful nowadays. This includes organic solar cells[4–10] and organic light emitting diodes (OLED).[11–13] Such devices are based on highly sophisticated molecular architectures comprising a variety of favorable properties that can be further tuned by chemical functionalization. Among them, most notably the selective absorption of light can be tuned mainly by varying energetic levels, for example, the HOMO-LUMO gap or the absorption energy of a charge transfer exciton; but also a large absorption cross-section due to large oscillator strengths and good charge transport properties are important. In particular, the latter can be further improved for electronic devices, which results in strongly enhanced conductivities upon doping.[14]

Organic field-effect transistors (OFET)[15–19] are another interesting family of devices. Although they are at present unable to compete with high-performance crystalline silicon technology due to inferior charge-carrier transport, they do offer certain advantages for inexpensive, large-area electronics applications, not least among them their low-temperature fabrication processes, which make them ideal candidates for manufacturing on flexible substrates. For this reason, organic field effect transistors in particular have attracted considerable interest in recent years and current research has produced individual transistor concepts for applications such as pixel driving in flexible displays,[20] logic circuitry[21–23] for RFID tags or smart clothing, biosensors, and other medical applications.[24–26]

1.2. Traditional Semiconductors: Limits of the Top-Down Approach

The success of semiconductor electronics and optoelectronics is in fact not only based on semiconductor materials but on a variety of compounds working together in different parts of an electronic device, including insulators, semiconductors, degenerately doped semiconductors and metals. Each of these serves a certain purpose.

Such a material classification is usually robust against variations in morphology and structure over some parameter range. On the other hand, upon downscaling from microstructures to nanostructures (which appears as a natural scaling sought-after in microelectronics industry) the properties of materials might

Dr. F. Ortmann, K. S. Radke, Prof. G. Cuniberti
Institute for Materials Science
Max Bergmann Center of Biomaterials and
Dresden Center for Computational Materials Science
Technische Universität Dresden
01062, Dresden, Germany
E-mail: Frank.Ortmann@tu-dresden.de
K. S. Radke, Prof. G. Cuniberti
Center for Advancing Electronics Dresden
TU Dresden
01062, Dresden, Germany
A. Günther, Dr. D. Kasemann, Prof. K. Leo
Institut für Angewandte Photophysik
TU Dresden George-Bähr-Str., 1, 01069, Dresden, Germany
Prof. K. Leo
4700 King Abdullah University of Science
and Technology (KAUST)
Solar & Photovoltaics Engineering Research Center
Thuwal 23955-6900, Kingdom of Saudi Arabia

DOI: 10.1002/adfm.201402334

deviate strongly from those in their bulk-phase. For example, differences in the coordination and atomic structure or built-in stress occur and may influence electronic properties. Additionally, quantum confinement effects play an important role, but also doping will be different in nanostructures compared to bulk materials due to effects of modified electronic screening. Such modifications might not be desirable. However, in fact, they cannot be avoided in a top-down approach that goes for further miniaturization with highly specialized (and costly) technological processing, which therefore lacks flexibility.

An alternative approach (bottom up) appears therefore as a suitable complementary strategy: to start with materials and fix their properties already at the level of the smallest structures (e.g., molecules) from which nanostructured assemblies can be constructed. This is where molecular and organic electronics step in.

1.3. Molecular Semiconductors: Bottom-up Research

When using molecules as basic building blocks, the research path is usually opposite to traditional semiconductors and follows a bottom up paradigm. The first step is the individual molecule, which is chosen according to a combination of specific needs (e.g., electron affinity, ionization potential, extinction coefficient, excitonic levels etc.). In a multistep approach, its properties are optimized (enhancement of solution processibility, self-assembly, morphology, intermolecular properties, etc.), which should lead to potentially efficient devices. Eventually one has to reiterate step one, if it turns out that the initial choice was not optimal.

A prototypical example for such bottom-up approach is a solution-processible organic semiconductor material, which has shown very high carrier mobilities in organic transistors, namely 6,13-Bis(triisopropylsilylethynyl)pentacene (TIPS pentacene).[27,28] It is based on the well-known small molecule pentacene, which is frequently employed as organic transistor material through evaporation of pentacene thin films.[29,30] The modified form, i.e., TIPS pentacene, is obtained by introducing side groups at the aromatic pentacene core that increase its solubility, while maintaining the ability to arrange in such a way that the π-conjugated molecular cores of adjacent molecules overlap, thus keeping the favorable transport properties of pentacene. Indeed solubility is obtained in common organic solvents and carrier mobilities reach about 2 cm^2/Vs for hole transport[31,32] and up to 6.8 cm^2/Vs for electrons in n-doped films.[33] This potentially allows for lower-cost processing technology such as printing techniques for high-performance materials.[34]

As illustrated in this example, the focus in molecular semiconductors is therefore often first on properties of single molecules, which can be studied either in solution (optical properties, electronic properties by cyclic voltametry), on surfaces (electronic properties by STM and related spectroscopy, conductive AFM etc.) or in solid phases (transport, dielectric properties of thin films, crystals, etc.). Investigating possible chemical modification is the second step that aims at improving functionality of the material in actual devices. This is an important difference to traditional (atom-based) semiconductors such as silicon, which lack such internal tunability and can only be modified by structural modifications of the respective atoms, which are alike such as in Si. This tunability by means of molecular functionalization is an intriguing perspective for materials design.

To fully understand this process, however, measurements have to be accompanied by respective theoretical models, which have to be adopted for the specific situation under study. Thereby, the mentioned advantages of molecular materials also pose a challenge for the theoretical description, since many characteristic energies (intrinsic or extrinsic interactions related to phonons, electrons, electron–phonon interaction,

Frank Ortmann is a senior researcher at the Institute for Materials Science of TU Dresden. He studied physics at the University of Jena, Germany, where he also received his PhD in 2009. After a postdoc at the Commissariat à l'énergie atomique et aux énergies alternatives (CEA) Grenoble as Marie-Curie Fellow and at the Catalan Institute of Nanoscience and Nanotechnology (ICN2) Barcelona, he joined TU Dresden in 2013 as senior researcher. Since 2014 he is head of an Emmy Noether young-investigator group.

Karl Sebastian Radke studied physics at the TU Dresden, Germany, where he is also doing his PhD studies on functionalization effects on the optical and charge transport properties of organic semiconductors and on doping effects in organic materials. He is part of the Center for Advancing Electronics Dresden.

Alrun Günther studied physics at Cardiff University, Wales, and graduated in 2012 with a first class Master in Physics (MPhys), the topic of her Master thesis being inorganic quantum well Hall sensors. She is now a PhD student at Technische Universität Dresden, Germany, focusing on vertical organic field-effect transistors as her main research area.

temperature, disorder, etc.) are on the same energy scale and cannot be easily separated. It is therefore necessary to develop efficient approaches capable of a reliable description, which can be linked to the specific material by means of first-principles simulations.

To reduce complexity in both experimental and theoretical studies, it is desirable to distinguish intermolecular and intramolecular properties. The present paper follows the spirit of this idea and will describe different theoretical approaches for modeling charge transport related to different experimental setups used to study and exploit the characteristics of molecular materials. In this paper, we will mainly distinguish molecular features that are defined on a single-molecular level and those arising from supramolecular assemblies. Both limits are commonly associated to closely adjacent research domains, namely Molecular Electronics and Organic Electronics, respectively. Thereby, a strong emphasis will be on the description of the electron–phonon interaction, which is crucial to molecular materials and imposes characteristic features for many experiments.

Several reviews have been dedicated to the charge carrier transport in bulk phases of molecular materials[19,35–37] (which are distinguished into oligomers and polymers[38] and its connection to the underlying material properties. In this paper, we will mainly focus on oligomers, that is, small molecules, but cover an extended range of devices and structures. The remaining part of the paper will focus on the two cases of molecular and supramolecular transport approaches, and is structured as follows. In Section 2, we briefly give a working definition of both research domains and illustrate the use of molecular materials in various devices by discussing a few illustrative examples where first concepts are introduced. Section 3 is dedicated to molecular properties and single-molecular transport, while Section 4 discusses supramolecular transport in more detail. In Section 5, we extend the description of supramolecular transport to disordered systems. Section 6 is focused on the determination of ab initio material parameters. Open challenges for current applications and perspectives are discussed in Section 7. The paper is concluded with a summary in Section 8.

2. Molecular Materials in Different Domains

2.1. Molecular Electronics and Organic Electronics

As the first of the mentioned research domains, we focus on Molecular Electronics. According to the rather narrow definition adopted here it is based on single (or very few) molecules as central components.[39,40] Molecular Electronics allows investigating molecular materials with unprecedented insight, which is certainly the biggest advantage of having a single molecule in an experimental setup. In recent years it has been driven to quite high sophistication, analyzing Kondo physics, Coulomb blockade[41,42] and other phenomena on the molecular scale. This was enabled by studying charge transport processes across nanojunctions, using the break junction technique or atomic-resolution techniques such as scanning probe spectroscopy and others[43] routinely. Conceptually, the molecules are assumed to be isolated from their surroundings, apart from a set of connected leads that are necessary to carry out quantum transport experiments (cf. **Figure 1**).

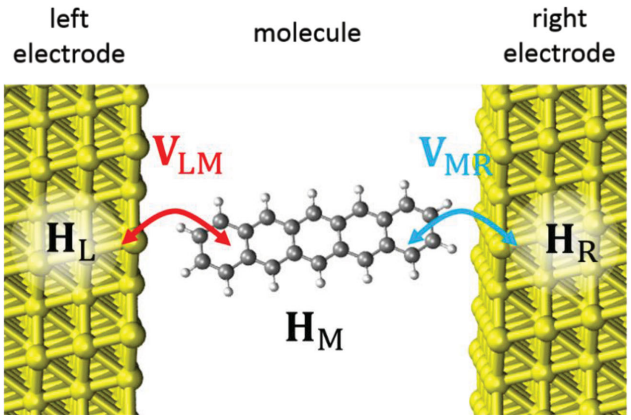

Figure 1. Setup for a single-molecular device, where a molecule is connected to two electrodes.

In contrast to this single-molecular picture, for the electronic and optoelectronics applications mentioned above (OLEDs, OFETs, organic solar cells), larger aggregates of organic molecules are used in devices going far beyond the molecular scale. Here, we use as working definition the term Organic Electronics, which considers also supramolecular effects.

2.2. Example 1: Molecular Rectification

Historically, ideas of molecular electronics could be found in the literature many decades ago. An important landmark is the seminal work of Aviram and Ratner on molecular rectifiers.[44] They proposed that a single molecule combining donor and acceptor moieties behaves like a diode when contacted electrically, that is, the asymmetric electronic properties manifest in a preference for either flow direction of the electrical current. The first asymmetric I–V curves for molecular films have been reported for Langmuir-Blodgett (LB) monolayers based on Z-β-(1-hexadecyl-4-quinolinium)-α-cyano-4-styryldicyanomethanide ($C_{16}H_{33}$-Q3CNQ) in the literature[45] and only in the late 1990s the unimolecular rectification was realized,[46] more than 20 years after its conception.

The requirement for the employed molecules to serve such a purpose was the presence of an electron donating unit and an electron accepting unit, which are separated by an insulating bridge in-between. In the initial proposal, tetrathiofulvalene (TTF) as donor was combined with tetracyanoquinodimethane (TCNQ) as acceptor,[44] giving rise to a true nanoscale diode of about 1 nm size.

The rectification mechanism involves inelastic tunneling from the acceptor to the donor unit, thus it is related to the emission of phonons in subsequent decay processes. Before and after this tunneling process the charge is assumed to be localized on either moiety due to the presence of an insulating bridge. In this model, localization results from electronic properties and does not require polaronic effects to step in, although they may occur. Comparing the characteristic energy for polaronic effects, that is, the reorganization energy λ (see

below) for TCNQ ($\lambda = 128$ meV)[47] with other relevant energies, it is probably smaller than the potential drop across the insulating bridge and of minor importance, so it is usually disregarded. Under this assumption and absence of dephasing, the transport can be assumed to be fully coherent and can therefore be tackled with the Landauer formalism,[48] which is introduced farther below in more detail. Figure 1 shows a separation into the subsystems molecule and leads (left and right) according to

$$H = H_M + H_L + H_R \tag{1}$$

which occurs in this formalism and which will be discussed in Section 3.

Here we finally note that beyond this diode architecture, the introduction of a third (or fourth) electrode as gate contact to the molecule represents a conceptual extension of the rectifier, where the size of the molecule becomes crucial, as it requires well defined electrodes and positioning in the sub-nm regime. This was first realized in a single-molecular transistor, shown by Park et al.[49]

2.3. Example 2: Zener Tunneling

Beyond the single-molecule devices and the molecular layer LB diodes, another device that is based on larger aggregates of organic material as active medium was realize with the Zener diode.[50] Such Zener diodes are important elements for voltage- and temperature stabilization and overvoltage protection in electrical circuits and essential to prevent parasitic current flow through non-selected cross-points in passive matrix memory arrays.[51]

Figure 2d shows the structure of the device, which is based on the pin diode concept, where each of the three active layers consists of small molecules. The p-type hole transport layer (HTL) was realized with MeO-TPD:F4TCNQ. The intrinsic interlayer (ILL) was Balq2:NPB, while the n-type electron transport layer (ETL) was Bphen:Cs. This stack was sandwiched between Al electrodes. The ILL thickness was varied between 5–11 nm while HTL and ETL thicknesses were both fixed at 50 nm.

Transport across the intrinsic layer in reverse operation mode can be directly tuned by the interlayer thickness. The transport mechanism has been analyzed in terms of its temperature dependence and barrier thickness (interlayer thickness plus depletion region).

Theoretically, one can approach this situation either by assuming fully coherent transport, as in the Landauer approach, or by assuming a hopping mechanism, for example, represented in a reduced density matrix approach.[52] Alternatively, more sophisticated treatments using polaron concepts, are possible (see below) but not necessary to analyze the situation qualitatively in the present case. Here, a one-dimensional model is employed, where each site (j) contains a HOMO and a LUMO orbital (with energies ε_j^s and with a gap $\varepsilon_j^{\mathrm{LUMO}} - \varepsilon_j^{\mathrm{HOMO}} = 3$ eV taken from experiment). In a minimal model, only electronic degrees of freedom of the HOMO and LUMO states are taken into account. Additionally to the molecular levels (and as an extension of the single molecule setup of the previous section), the intermolecular coupling t is introduced and assumed being constant for simplicity. The Hamiltonian thus reads

$$H_1 = \sum\nolimits_{s=H,L}\left[\sum\nolimits_j \left(\varepsilon_j^s a_{s,j}^\dagger a_{s,j} + t a_{s,j}^\dagger a_{s,j+1} + t a_{s,j+1}^\dagger a_{s,j}\right)\right] \tag{2}$$

The on-site energies $\varepsilon_j^{\mathrm{LUMO}}$ change over the channel encoding the build-in field arising from the pin structure even at zero bias. Application of external source–drain voltage adds additional local potentials.

The electronic transfer from HOMO to LUMO states in the Zener mechanism is described with interband coupling terms $t_k^{\mathrm{H\text{-}L}}$ between frontier orbitals

$$H_2 = \sum\nolimits_j \left(t_1^{\mathrm{H\text{-}L}} a_{\mathrm{H},j}^\dagger a_{\mathrm{L},j+1} + t_2^{\mathrm{H\text{-}L}} a_{\mathrm{H},j}^\dagger a_{\mathrm{L},j+2} + \mathrm{h.c.}\right) \tag{3}$$

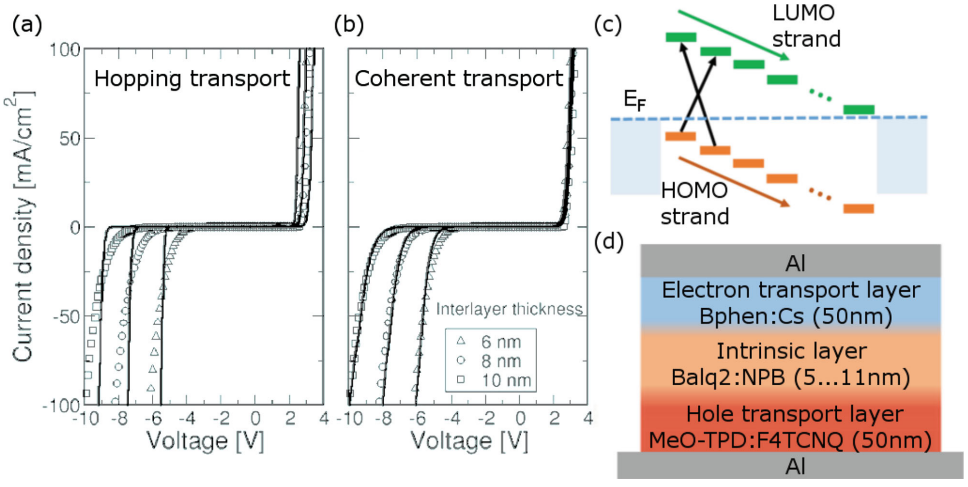

Figure 2. a,b) Measured (symbols) and calculated (lines) *I–V* characteristics in an organic Zener diode. c) Ladder model of the electronic structure with the built-in voltage reducing the HOMO-LUMO gap of adjacent molecules. d) Device design. Adapted with permission.[50] Copyright 2010 American Chemical Society.

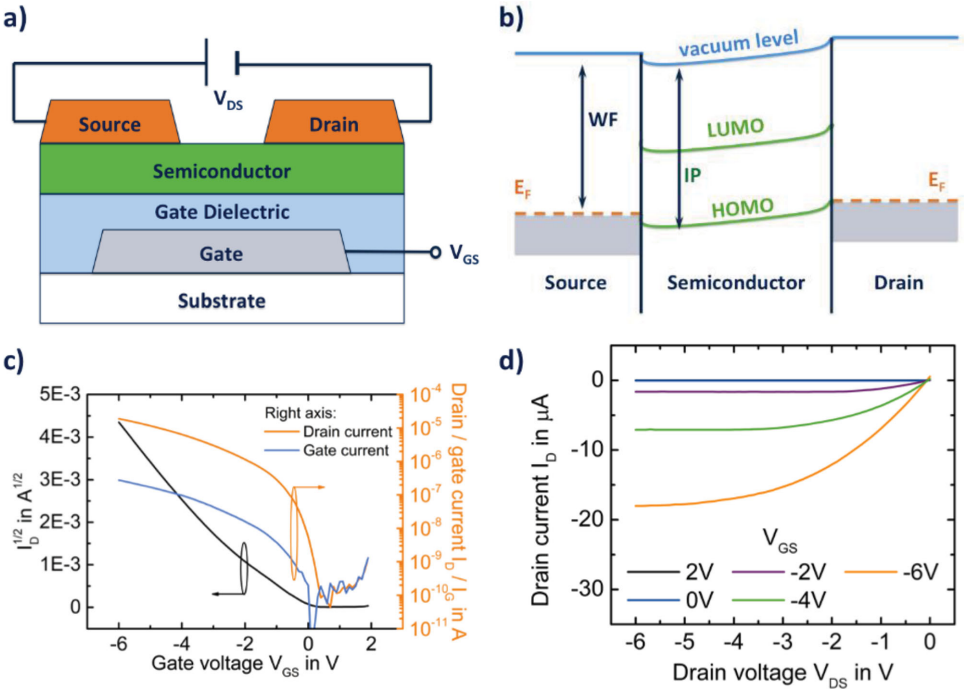

Figure 3. Schematic of a) a bottom-gate, top-contact OFET with b) energy level diagram, c) transfer characteristics, and d) output characteristics of a p-type OFET.

including nearest neighbor ($k = 1$) and next nearest-neighbor terms ($k = 2$).

Figure 2 compares the analysis of the experimental results assuming coherent or incoherent transport regimes. Both approaches are able to simulate qualitatively the observed I–V characteristics, while the analysis does not attempt quantitative agreement. The thickness dependence of the breakthrough voltage (at negative bias) is related to the energy difference of HOMO and LUMO levels of neighboring molecules (or more distant molecular pairs), that is, under reverse operation mode, the built-in voltage (Figure 2) is enhanced by the external field which triggers HOMO–LUMO tunneling. For larger ILL thickness, the onset occurs at larger negative voltages as it drops over longer distances. This effect can be described in a similar way based upon both transport regimes.

On the other hand, the weak ILL-thickness dependence under forward voltage is related to the alignment of the first molecular state with the Fermi level of the left electrode (see Figure 2). Further voltage increase leads to a reduction of the built-in field and level alignment of the molecular states in the ILL thus increasing the current at positive voltages. This example shows that for a rough understanding only a few empirical parameters are required while the effort to detail the understanding is considerably larger.

2.4. Example 3: Carrier Transport in Bulk Materials

In contrast to the above examples, where we have discussed single molecule devices, larger aggregates with self-assembled monolayers, or thin films in the Zener diode geometry, we focus now on bulk phases. For a large part of applications based on molecular materials, the limit of bulk material is even more relevant. We turn now to this limit for supramolecular assemblies, where intermolecular interaction plays an additional role. Accordingly, bulk phases of organic matter are classified by different morphologies of materials, ranging from molecular single crystals[19,36] via polycrystalline[37] and thin film phases to amorphous morphology.

The transport properties and in particular the charge carrier mobilities of materials in bulk phases are typically investigated by two main experimental methods: Time of flight measurements (TOF) and organic field-effect transistors (OFET). However, while the mobilities extracted from TOF measurements strictly describe the bulk transport scenario, the field-effect mobilities extracted from OFET measurements are generally much higher, owing to the significantly higher charge carrier density in the conductive channel, and generally describe the transport in the thin film phase for polycrystalline and amorphous materials.

The standard organic transistor (**Figure 3**a) follows the well-known MISFET concept in the sense that it is a field-effect transistor based on a metal-insulator-semiconductor geometry comprising a semiconductor layer, an insulator (also called the gate dielectric), and three electrodes: an injecting contact (the source), a collecting contact (the drain), and a control electrode (the gate). These can be arranged in different geometries (see study in the literature for a more detailed description),[53] the basic functional principle of the OFET however is the same for all geometries: By applying a voltage to the gate electrode (the source-gate voltage V_{GS}), charge carriers are accumulated at the interface between the semiconductor and the gate dielectric, thus forming a thin sheet of mobile charges within the first few monolayers of the semiconductor material near

the interface. Application of an additional voltage between the source and drain contacts (V_{DS}) causes a current to flow through this highly conductive region (the channel) near the gate dielectric interface, which can be collected at the drain and is thus termed the drain current I_D. The magnitude of I_D is controlled by the conductivity of the channel and thus by V_{GS}.

While the charge transport mechanisms in organic semiconductors are generally different from those of inorganic semiconductors, as illustrated farther below, the OFET can still be described by the standard MOSFET formalism:

$$I_D = \frac{\mu C W}{L}\left((V_{GS} - V_{th})V_{DS} - \frac{V_{DS}^2}{2}\right) \quad (4)$$

for $|V_{GS} - V_{th}| > |V_{DS}|$ (linear regime) and

$$I_D = \frac{\mu C W}{2L}(V_{GS} - V_{th})^2 \quad (5)$$

for $|V_{DS}| > |V_{GS} - V_{th}| > 0$ (saturation regime), where μ is the charge carrier mobility, C the capacitance of the gate dielectric, W and L the width and length of the conductive channel and V_{th} is the so-called threshold voltage of the transistor, which (unlike in the standard MOSFET model) is defined as the gate voltage at which I_D can first be described by Equation 4. Below V_{th} (the subthreshold region), I_D is exponentially dependent on V_{GS}.

From Equation 4 and 5 it is possible to extract the charge carrier field-effect mobilities for the linear and saturation regimes:

$$\mu_{lin} = \frac{L}{CWV_{DS}}\frac{\partial I_D}{\partial V_{GS}} \quad (6)$$

for $|V_{GS} - V_{th}| > |V_{DS}|$ (linear regime) and

$$\mu_{sat} = \frac{2L}{CW}\left(\frac{\partial\sqrt{I_D}}{\partial V_{GS}}\right)^2 \quad (7)$$

for $|V_{DS}| > |V_{GS} - V_{th}| > 0$ (saturation regime).

High mobilities in organic semiconductors can be achieved either through highly ordered polycrystalline materials or organic single crystals. Recent works of Yuan et al. and Okamoto et al. have produced field-effect hole mobilities in polycrystalline organic semiconductors of 43 cm^2/Vs[54] and 21 cm^2/Vs,[55] respectively, both measured at room temperature in thin films produced either from solution or thermal evaporation. While the result of Yuan et al. in particular exceeds even the highest hole mobilities achieved in organic single crystals, which currently range around the 20 cm^2/Vs mark[56,57] (with electron mobilities one order of magnitude lower,[58,59] organic single crystals are nonetheless very successfully employed not only to produce high-performance OFETs, but also to understand the functional principles of OFETs in much more detail, since effects such as band-like transport[57,60] can only be observed in organic single crystal transistors. Such transistors are often fabricated by laminating previously grown crystals onto a bottom gate structure, which offers the additional advantage of investigating OFET characteristics in a geometry where the quality of the organic semiconductor is approximately constant, so that, for example, the phenomenon of contact resistance can be distinctly separated from effects due to morphological differences in the semiconductor around the electrodes.[61] Unfortunately, these more complex fabrication methods employed to create organic single crystal transistors will most likely not be suitable for integration into mass manufacturing, so that OFETs intended for consumer applications rather than research generally use amorphous or polycrystalline semiconductors. The understanding of charge carrier transport in such amorphous and polycrystalline material systems must consequently form a vital part of organic semiconductor research, just as transport within single molecules must be understood in more detail.

3. Describing Molecular Scale Conduction

3.1. Basic Approach to Electronic Transport

A single molecule placed between electrodes (as in the above examples, cf. Figure 1) is similar to any other nanoscale object, such as a nanodot, in that strong quantum confinement effects lead to a quantization of levels with large energetic separation between orbitals. In contrast to nanodots however, a molecular structure is very specific and atomically precisely defined, not leaving any doubt about its chemical formula and structure, which results from synthesis. On the contrary, conformational variety might be larger for molecular systems, particularly for large molecules owing to side group dynamics, and so forth.

While this effect is minor for simple molecules, such as H_2,[62] benzene,[63] or C_{60},[49,64] which are interesting more from a fundamental point of view than for actual applications, larger molecules comprising higher functionality are more flexible but can be attached more strongly to noble metal surfaces with thiol groups.[65,66] A stronger link to the metal electrodes has the advantage that possible unwanted conductance variations due to structural fluctuations are minimized, which is the way to go for a better control towards nanoelectronics applications.[67] In any event, the dynamics of the molecules has to be taken into account in the modeling of single-molecule electronics.

The basis for such modeling are metal/molecule/metal setups which are denoted two-terminal devices, because electrons can only enter or leave through the two electrodes. It is possible to extend this idea to many electrodes (terminals) that contact a given molecule at different points, as in transistor configurations,[41,49,68,69] and to further increase the complexity and level of integration. It is not the aim here to describe the development towards higher integration, but to point out the basic theoretical framework to tackle such transport problems for which we focus on the simplest geometry.

Figure 1 shows the usual setup in an idealized form, where the isolated molecule is sandwiched between source and drain electrodes. Accordingly, the molecule is distinguished from the leads, which is represented in a block structure of the Hamiltonian

$$H = \begin{pmatrix} H_L & V_{LM} & 0 \\ V_{LM}^{\dagger} & H_M & V_{MR} \\ 0 & V_{MR}^{\dagger} & H_R \end{pmatrix} \quad (8)$$

where H_L, H_M, and H_R describe the isolated left lead, molecule, and right lead, respectively. The quantities V_{LM} and V_{MR} describe the coupling terms between molecule and lead blocks.

An adequate transport description can be achieved within the Landauer approach, relating the conductance of such a sample to its electron-transmission probability.[70,71] This approach assumes a fully coherent transport situation, that is, the transport (tunneling) distance between electrodes is significantly smaller than the phase coherence length ℓ_{ph}. Indeed the latter quantity is a highly relevant parameter for the present problem as its size can be reduced by a variety of decoherence processes. Such decoherence effects may arise from electron–phonon coupling, electron-electron interaction, or other coupled internal or external degrees of freedom that lead to phase randomization. This would be increasingly relevant in the case of additional molecules in the surrounding and for longer charge transport length (see Section 4).

In the simplest case, when no scattering takes place, ballistic transport is observed in metallic chains, with ideal conductances reaching multiples of the quantum conductance G_0. In the present section, we rather focus on situations including elastic scattering, which happens when the lead states encounter a molecule (which is to be probed) and do not propagate freely. Such a scattering obstacle reduces the conductance, which is observed in the case of transport through single molecules. Still transport can be coherent in this case because the number of potential inelastic scatterers that may lead to decoherence is strongly reduced in experiments.

One can therefore use the general formalism of mesoscopic transport,[48] in which the current through a nanoscale system is written for non-interacting electrons as

$$I = \frac{2e_0}{h} \int^{T}(E)\left[f_l(E) - f_r(E)\right]\mathrm{d}E \quad (9)$$

Here the transmission $T(E)$ takes into account the number of transmitting channels and can be written as

$$T(E) = \mathrm{Tr}\left[\Gamma_L \mathcal{G}_M(E)\Gamma_R \mathcal{G}_M^{\dagger}(E)\right] \quad (10)$$

where

$$\mathcal{G}_M(E) = \left((E + i\eta)\mathrm{I} - H_M - \Sigma_L - \Sigma_R\right)^{-1} \quad (11)$$

and

$$\Gamma_{L/R} = i\Sigma_{L/R} - i\Sigma_{L/R}^{\dagger} \quad (12)$$

are related to the self energies $\Sigma_{L/R}$ due to the left/right contacts and describe the electrodes and their coupling to the molecule.

The integration over the bias voltage V is a key feature of the involved physics and leads to a stepwise increase of the tunneling current when additional transport channels between electrodes and molecule become accessible. On the other hand, it is also interesting to consider the conductance $G = \mathrm{d}I/\mathrm{d}V = \frac{e_0^2}{h}\int^{T}(E)\left[-\frac{\partial f(E)}{\partial E}\right]\mathrm{d}E$ and its derivative $\mathrm{d}^2I/\mathrm{d}V^2$, which have characteristic features at energies related to excitation levels of the system. Such measurements that probe the voltage dependence are referred to as tunneling spectroscopy, which is used to study the excitation spectrum of the molecule under investigation.

3.2. Dephasing and Surrounding

While the above example discussed a fully coherent transport regime and did not consider explicitly the effect of phase breaking effects, it is interesting to consider the occurrence of these effects. We do this here for the case of a molecular junction by connecting to the above discussions. Indeed, there has been some emphasis on this issue in recent literature with focus on different organic materials, including the prototypical 1,4-benzenedithiol molecule,[72] simple benzene in varying configuration (ortho, meta and para),[73] polyanilin molecular wires,[74] or para-phenylene vinylene- (PPV) and pyrrole-oligomers.[75]

Such studies were strongly motivated by experimental evidence that a transition occurs between coherent tunneling and hopping motion as a function of the length of an aromatic molecular wire. In fact, if the transport length is larger than ℓ_{ph}, coherent processes are cut off. This transition directly manifests in the length dependence of the resistance, changing from an exponential increase to a linear increase with transport length.[76]

Similar effects have been discussed in donor–bridge–acceptor systems in solution. In such cases, the transition behavior can be related to the surrounding, which decoheres the system under study.[77,78] For an isolated molecule considered here this is not obvious as the interaction with the surrounding is ultimately reduced to the electrodes only. In any event, as the geometry is not strictly frozen, the molecular motions (e.g., slow vibrations) lead to a fluctuating electronic structure.

Different approaches to consider this electron–phonon coupling have been presented. Among these we mention the conceptually relatively simple D'Amato-Pastawski model,[79] which expands on the original idea of the Büttiker probes[80] and which has been applied to molecular conductors before.[81] The model consists of a two-terminal setup, as described in Hamiltonian 1 supplemented with a set of local probes in the central region of the junction (see Figure 2a). These probes do not act as terminals, that is, the current through them is zero; but they give rise to some phase randomization. These are included as self energies $\Sigma_{B,j}$ for the position j according to

$$\mathcal{G}_M(E) = \left((E + i\eta)\mathbf{I} - H_M - \Sigma_L - \Sigma_R - \sum_{j=1}^{J}\Sigma_{B,j}\right)^{-1} \quad (13)$$

where J is the number of connected reservoirs (probes) and $\Gamma_j = i\left(\Sigma_{B,j} - \Sigma_{B,j}\right)$ can be understood as a phenomenological

dephasing energy, which may arise from electron–phonon coupling for instance. We use a constant Γ to tune such an interaction as an effective dephasing parameter.[75]

The effective transmission in this model consists of direct coherent transmission processes from the left to the right lead $T_{L,R}$ and incoherent ones which pass through the n-th probe. The total transmission can be expressed as

$$T_{\text{eff}} = T_{L,R} + \sum_{n,n'=1}^{N} T_{L,n} W_{n,n'}^{-1} T_{n',R} \tag{14}$$

where the incoherent contribution involves the so-called Markov matrix $W_{n,n'}$ that is built from individual transmission processes $T_{n,n'}$ between the probes n and n', which are treated independently as a standard two-terminal problem.

Figure 4 shows the dependence of the transport parameters transmission and resistance on the number of PPV-based oligomer units as well as on the dephasing parameter Γ. We observe some remarkable features. First, for a single unit decoherence does not play a significant role throughout the large range of Γ values considered. In contrast, as PPV length increases, it becomes gradually more important such that beyond 3 units, even the smallest Γ studied renders transport mostly incoherent. The corresponding resistance in Figure 4c shows that dephasing can be described as a crossover from exponential to linear resistance.

Unfortunately, in this model it is not straightforward to connect the empirical parameter Γ to a microscopic picture of electron–phonon coupling events in the fictitious probes, but it works very well as a minimal model for illustrating the transition due to decoherence effects.

3.3. Electron–Phonon Interaction

3.3.1. Basic Effect of Electron–Phonon Coupling

A more formal way to describe that a change in geometry entails a change in the electronic structure and to introduce the electron–phonon coupling microscopically is by performing a simple Taylor expansion of the molecular electronic levels. This can be formulated either with respect to atomic coordinates R_i or vibrational coordinates X_λ, respectively:

$$\varepsilon = \varepsilon_0 + \sum_i^M r_i \cdot \nabla_{R_i} \varepsilon(\{R\}) = E_0 + \sum_\lambda^N x_\lambda \frac{\partial \varepsilon(\{R\})}{\partial X_\lambda} \tag{15}$$

where the displacement vectors r_i for atom i and the displacement coordinate x_λ along the mode vector λ have been introduced. Both are related by a simple change of the basis. Usually one restricts to first order changes, assuming that they are the dominant contributions. The relevant coefficients

$$g_\lambda = \frac{\hbar}{\sqrt{2}(\hbar\omega_\lambda)^{3/2}} \frac{\partial \varepsilon}{\partial X_\lambda} \tag{16}$$

are the electron–phonon coupling constants, here defined in a dimensionless fashion.[82] Using this definition, they correspond to the standard formulation of electron–phonon coupling in the Hamiltonian

$$H = \sum_M \varepsilon_M a_M^\dagger a_M + \sum_{M,\lambda} g_{M\lambda} \hbar\omega_\lambda a_M^\dagger a_M \left(b_\lambda^\dagger + b_\lambda\right) + \sum_\lambda \hbar\omega_\lambda b_\lambda^\dagger b_\lambda \tag{17}$$

similar to the Holstein Hamiltonian.[83,84] The first term is purely electronic (here restricted to a single molecule), while the second and third terms describe the electron–phonon coupling and the phonon energy, respectively.

The molecules under scrutiny usually exhibit a wide distribution of vibrational modes from high-energy C–H stretch modes to low-frequency collective vibrations, where the whole molecule bends (e.g., in butterfly modes). Among such modes, the coupling to the electronic levels is not equal and it is not a priori clear which of the modes couple strongly and which have only minor influence on the electronics, as this depends on the vibrational pattern and the shape of the molecular orbital. Having stated this, however, it is clear that in the case of orbitals that are localized on a certain part of the molecule, the vibrations involving atoms in this part are more relevant than others. Ultimately, most modes do not couple to the first order of x-displacements for symmetry reasons and only a few modes typically couple strongly. The above example of TIPS pentacene, where the frontier orbitals are localized on the molecular core, that is, not on the side groups, is very illustrative. Vibrational motions in these side chains do not noticeably influence the orbital electronics.

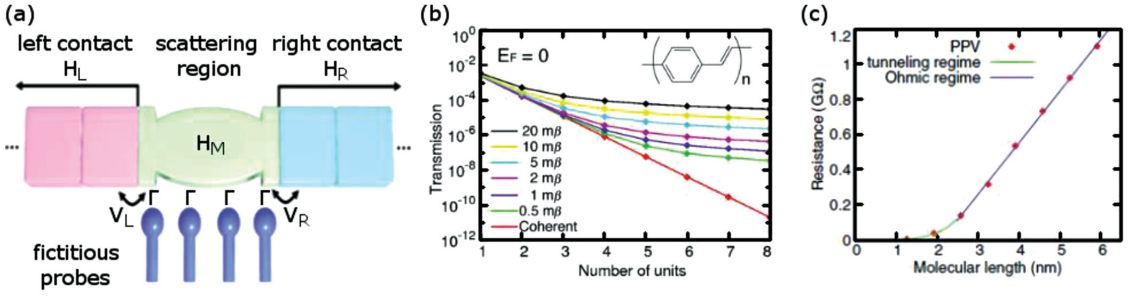

Figure 4. a) Transport configuration with left and right contacts coupled to a trapped molecule (described by H_M). The surrounding influences the molecular levels through a self-energy Γ. b) Transmission function including both coherent and incoherent transport processes by varying Γ from 20 mβ down to 0.5 mβ ($\beta = -2.7$ eV is the C–C transfer integral between aromatic carbons in the molecule). c) Resistance as a function of molecular length showing crossover from tunneling to Ohmic behavior as triggered by decoherence. Adapted with permission.[75] Copyright 2012 American Physical Society.

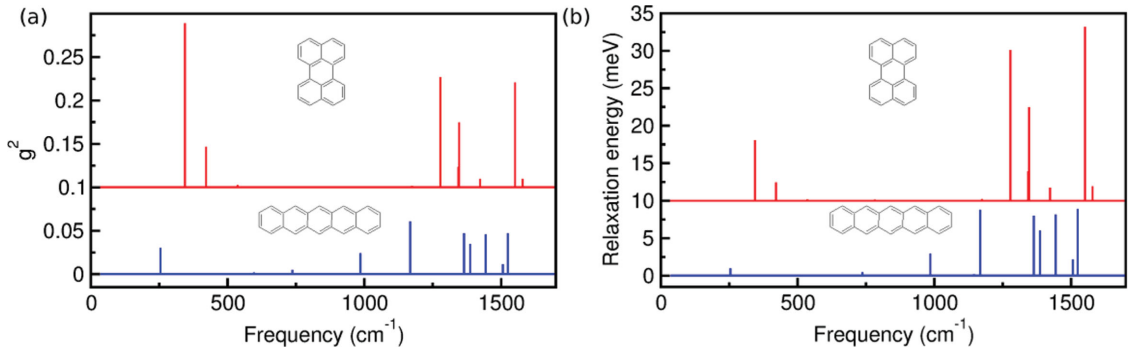

Figure 5. a) Squared electron–phonon coupling constants g^2 (HOMO) plotted versus phonon frequency for perylene and pentacene. b) Specific contribution to the (HOMO) relaxation energy $E = \omega g^2$ upon ionization. Calculations were performed with the B3LYP exchange-correlation functional and 6–311 G (d,p) basis set. Frequencies were corrected by a factor 0.967[201] and g^2 were corrected by the inverse factor.

3.3.2. Limits of the Model of Linear Electron–Phonon Coupling

One should also mention that Equation 15 is valid only if the geometry change is small enough. While this is usually fulfilled for most intramolecular vibrations and small molecules, functional side groups might rotate relatively freely around a chemical bond (torsional mode).[85] Also, more complex changes in the geometry observed for instance in quasi-static conformational changes influence electrical properties[86,87] or optical properties[88] of single molecules, but cannot be described in the Holstein model. Additionally, conformational changes can be more involved or one observes a molecular switching behavior,[86,89] which would be another example where this linear expansion is expected to break down.

These latter cases are different because of additional deviations from the harmonic potential (which we have tacitly assumed to be present for all atomic displacements in Hamiltonian 17) that occur for large displacement vectors. Such anharmonic effects entail phonon-phonon interaction and are central to the question of decoherence effects but rarely studied.

In contrast to traditional semiconductors, the electron–phonon couplings g entering Equation 17 are, generally speaking, not weak in molecular systems and not treatable within perturbative approaches. One of the reasons is the softness of organic matter and the presence of associated low-frequency vibrations which favors large g values. We note that the small frequencies appear as a prefactor in the denominator in Equation 16. Some examples for typical values will be given below. As a consequence of the size of the electron–phonon couplings, this interaction needs to be included non-perturbatively in electron transport theory.

3.3.3. Materials and Values

In this section we present typical material parameters of the electron–phonon couplings which are central to molecular materials. We first focus on aromatic hydrocarbons and consider local coupling parameters. **Figure 5**a displays a distribution of coupling constants g^2 over vibrational frequency, comparing pentacene and perylene. It shows contributions from high-frequency modes between 1000 cm^{-1} and 1600 cm^{-1} and one or two modes below 500 cm^{-1}. Not all modes (in total $3N$-6, where N is the number of atoms) contribute because of the symmetry of the orbitals and the symmetry of the modes, which imposes selection rules. The absolute values of the coupling constants vary over many orders of magnitude with the largest values on the order of 0.5 or even 1 (see Figure 5a).

Because of its importance and to gain more insight into what is at the origin of such electron–phonon couplings and in some tendencies observed for the values, we briefly discuss an illustrative example. **Figure 6** shows the evolution of a particular phonon mode for the oligoacenes family when the molecule increases in size. The mode is a ring-breathing mode of the innermost aromatic ring. The corresponding electron–phonon coupling constant is plotted in **Figure 7**. When increasing the size of the molecule from benzene to heptacene, the coupling constant changes smoothly but strongly. It even changes its sign with a minimum of its modulus for anthracene. As the related HOMO state is spanning the whole molecule, different parts of the molecule must contribute with different signs, leading to a compensation effect (resulting in $g \approx 0$) for anthracene. Indeed, for the smallest molecule, benzene (not shown), only the central core contracts for this mode, which due to a strong

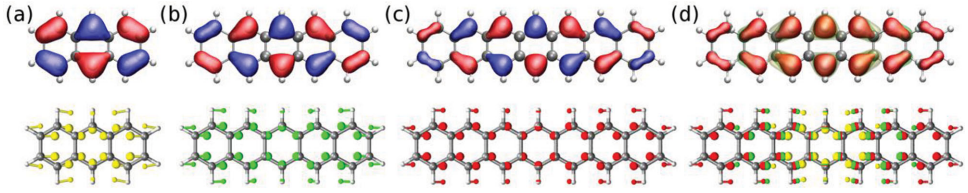

Figure 6. HOMO states and mode vectors of vibrational breathing mode for a) anthracene, b) pentacene, and c) heptacene. The vibrational modes are similar for all oligoacens showing two main features: i) a contraction of central ring and ii) a translation of outer rings toward the inner ring in phase with (i). d) superposition of cases (a–c).

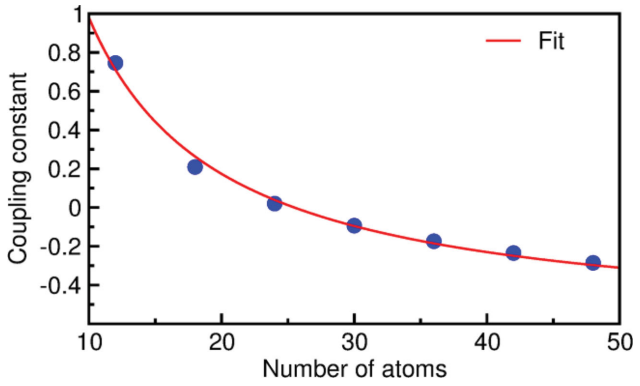

Figure 7. The electron–phonon coupling constants for the vibrational breathing modes of the oligoacenes (cf. Figure 6) exhibits a smooth dependence on the oligoacene length from benzene to heptacene (number of atoms are displayed). The lowest value for $|g|$ is obtained for anthracene ($n = 24$). Fit: $g(n) = 16/n - 0.63$.

confinement of the HOMO leads to a large coupling constant $g = 0.74$. Figure 6 shows that the motion of the central ring is gradually reduced with molecule size within the oligoacenes series up to heptacene (cf. comparison in Figure 6d), leading to a reduction of its contribution to the coupling constant. At the same time, the motion of the outer rings gains importance with negative contributions to g, which finally leads to the observed sign reversal in the coupling.

Besides the coupling parameter of an individual mode, the entirety of modes, which can be expressed as an integral or effective coupling, has some relevance for transport, as discussed below. One defines the reorganization energy as

$$\lambda = \sum_i g_i^2 \hbar\omega_i \tag{18}$$

which is a direct measure of the geometrical relaxation of a molecule upon charging.

Figure 8 shows the reorganization energies for the oligoacenes family, from benzene to heptacene in comparison to perylene, coronene, and diindenoperylene, to contrast linear and more planar molecules with equal numbers of rings.

One first observes a clear tendency within the oligoacenes family that the larger the molecule, the smaller the reorganization energy. Similar results have been obtained before for holes in the oligoacenes series from naphthalene to pentacene.[90] Besides such a trend within the family, the comparison to perylene shows that the number of rings is not the only relevant parameter that determines the reorganization energy, that is, the mere extension of the wave function is only one among many factors. This is similarly seen when comparing heptacene and coronene, which has almost twice the reorganization energy for the same number of aromatic rings.

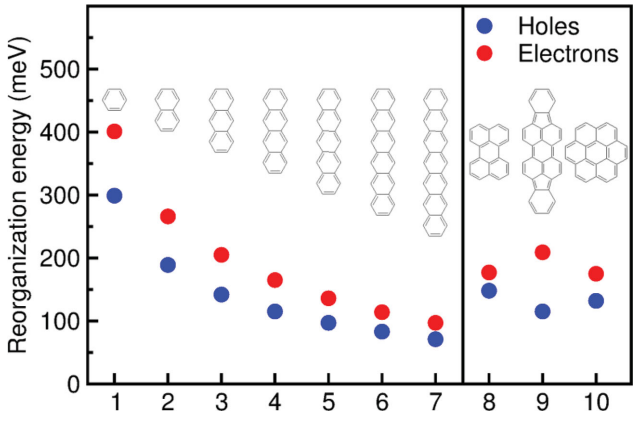

Figure 8. Electron and hole reorganization energies for oligoacenes (left panel) and perylene, diindenoperylene and coronene (right panel).

Another effect is also interesting when comparing to diindenoperylene. The difference between electron- and hole reorganization energies (which tends to vanish for larger polyacenes), can be strongly enhanced by the indeno group, which, as a 5-membered ring, modifies the aromaticity and leads to twice as large values for electrons than for holes.

3.4. Electron–Phonon Coupling Effects at the Molecular Scale

3.4.1. Modelling Inelastic Transport Effects for Molecular Junctions

The study of vibronic excitations of molecules by means of electrical measurements and tunneling spectroscopy dates back almost 50 years. In 1966, Jaklevic and Lambe[91] observed a connection between intramolecular vibrations of molecules hosted in oxide-based tunneling junctions and peaks in transport signatures occurring at increasing voltages across the junctions and they have related both through inelastic tunneling effects. These spectra include information which is characteristic for the molecules under study and the technique is known as Inelastic Electron Tunneling Spectroscopy (IETS). Such inelastic effects can be related to additional transport channels in the tunneling problem discussed in Section 3.1 for purely electronic degrees of freedom. An excellent review about IETS can be found in the literature.[92]

The simplest way to include phonons in the molecular system is given by the Holstein-type model in Equation 17. In principle, this may include both genuine intramolecular vibrations as well as vibrational modes related to the position and orientation of the molecule in the junction. Both can be relevant.

Early theory to describe the effect of the electron–phonon interaction on transport[93,94] is based on Fermi's Golden Rule expression for incoming and outgoing waves which are evanescent in the tunneling region. As perturbation, one uses the change in the molecular potential due to the coupling to vibrational modes, which modifies the Mth orbital energy through $g_{M\lambda}$ in Equation 17. As a result of the vibronic coupling, one observes additional peaks in the second derivative of the current with respect to the voltage V[94]

$$\frac{\partial^2 I}{\partial V^2} \propto \int^d K\, dK'\, M(E, E - e_0 V, K, K')\, \delta(e_0 V - \hbar\omega) \tag{19}$$

This expression relates the amplitude of the signal at resonant energies $(e_0 V = \hbar\omega)$ to matrix elements M between incoming (K) and outgoing (K') states through a convolution of all such states at a given Fermi energy. It should be mentioned, however, that such a perturbative result is altered when the coupling between the lead states through the molecule is no longer small. A more sophisticated treatment is based on the non-equilibrium Green's function technique and the self-consistent Born approximation.

As a result, both the amplitudes of the IETS signals and the line shapes may change as discussed in another study.[95] On the other hand, the vibrational energies, that is, the feature positions, are unchanged by varying theoretical details, which allows to relate them to true vibrational modes, either of purely molecular character or modes related to molecule–surface bonds.

Features as described above should be observable when the signal is strong enough and the energy resolution is high enough. However, thermal energy leads to smearing of electronic energies, which increases the intrinsic broadening. First results from electrical measurements of trapped molecules could not resolve very specific features for the molecules under investigation and average signals from many molecules measured simultaneously have been obtained.

3.4.2. Experimental Observation of Inelastic Quantum Transport

The first paper reporting on spectroscopic investigation of a single molecule [96] could relate the observed IETS features to C–H stretch modes by measuring the isotope effect. These effects have been further studied for instance in alkanethiol self-assembled monolayers[97] or alkanes [98,99] where a variety of vibrational modes of the studied molecules could be identified.

Other groups have extended the complexity to three terminal setups and the first single molecule transistor was realized by Park et al.[49] Such experiments have also a specific vibrational signature of the molecule which manifests in $\mathrm{d}I/\mathrm{d}V$ peaks. An intriguing comparison between C_{70} and C_{140} molecules (covalently linked C_{70} by design) in single molecular transistors revealed genuine intramolecular vibrations with frequencies as low as 11 meV.[100]

All these experiments (and many more) demonstrate that, besides the identification of a single molecule present in the junction, its orientation and interaction with electrodes can be studied.[40] However, significant variations in the molecular structure influence the transport result such that a single measurement often cannot describe the system in an adequate way but statistical approaches are necessary in experiment and also theory. This is so because in the measurement one cannot control the contact on an atomic scale, such that fluctuations lead to a set of possible configurations, which are best represented in a statistical way.

In praxis, the experiments usually require ultra-high vacuum conditions, ultra-low temperatures, and cleaning procedures to study ultimately single molecular properties, but also fundamental studies of quantum coherence and decoherence mechanisms are in principle possible. Indeed, studying these effects is highly important to understand functionality of molecular materials in actual applications.[101] The importance of supramolecular effects in such applications will be discussed below.

4. Describing Supramolecular Effects

4.1. Electronic Properties beyond Single Molecules

In this section, we will discuss bulk phases of molecular materials. As stated in the introductory part, intermolecular interaction will play a major role, which is seen in the strong impact that material morphology has on transport properties, as for instance in amorphous and single crystalline phases. We therefore have to expand on the above description of purely intramolecular properties. One important extension to the Hamiltonian (17) is the inclusion of intermolecular (so-called non-local) terms for electrons and phonons. The extended Hamiltonian reads

$$H = \sum_{MN} \varepsilon_{MN} a_M^\dagger a_N + \sum_{M,N,\lambda} g_{MN\lambda} \hbar\omega_\lambda a_M^\dagger a_N \left(b_\lambda^\dagger + b_\lambda\right) + \sum_\lambda \hbar\omega_\lambda b_\lambda^\dagger b_\lambda \tag{20}$$

The first term describes the electronic coupling ε_{MN} between different molecular orbitals M and N of adjacent molecules or more distant neighbors, while the corresponding non-local electron–phonon coupling terms (Peierls-like coupling) are described by $g_{MN\lambda}$ for all modes λ. We discuss the electronic terms first.

Absolute values for ε_{MN} are rather small compared to, for example, inorganic semiconductors, that is, they are typically one order of magnitude smaller and rarely exceed 100 meV. Besides the absolute values of the transfer integrals, which are characteristically small, electronic anisotropy is ubiquitous in single-crystalline organic semiconductors, as proven by first principles calculations,[85,102–110] by angle-resolved photoelectron spectroscopy (ARPES),[111–118] and also by low-temperature measurements of the carrier mobilities,[119] and references therein. This anisotropy is intimately related to the molecular packing in the crystal structure. Often one encounters a herringbone fashion for this packing, that is, a 2D plane of molecules arranging face to edge. These planes are stacked in the third direction, giving rise to an in-plane vs out-of plane anisotropy with larger electronic couplings ε_{MN} in the plane. But even within the herringbone planes, mobility anisotropy can be observed frequently.[120] Other molecular arrangements include quasi-one dimensional stacks of molecules, such as in guanine crystals, which implies corresponding 1D transport characteristics at low T.[121]

In polycrystalline materials it is usually assumed that, due to a random orientation of crystalline grains (see, e.g., measurements for pentacene),[122] the effects of direction dependence of transport are averaged out, which is also confirmed experimentally. The same applies to amorphous morphologies.

In order to study fundamental issues of carrier transport in bulk organic matter, it is therefore necessary to study ultrapure single crystals with a strongly reduced number of defects, as otherwise the intrinsic properties would be masked and a detailed characterization of defects (which in most cases is not accessible) would be necessary in the experiments. For ultraclean crystals, all parameters ε_{MN} in Hamiltonian (20) that are related by translational symmetry, are equal. In this case, one can analyze experimentally the band dispersion of such crystals by means of ARPES,[111–117] which also allows to study effects of chemical substitution.[123]

On the theoretical side the parameters can be obtained by first principles simulations as described in Section 6. Beyond such fundamental questions related to single-crystalline materials, disordered morphologies can be described with static disorder being encoded in the energies ε_{MM} (local) and ε_{MN} (non-local) in various ways either in an uncorrelated way or by taking correlations into account. Disorder models can include grain boundaries or longer ranged potentials that describe charged defects for instance. Also the substrate influence can be modeled in such a way.

4.2. Non-local Electron–Phonon Coupling

4.2.1. General Description

Besides such static disorder, dynamic aspects and energetic fluctuations are encoded in the local and non-local electron–phonon couplings. Even in ultrapure crystals the transfer integrals are not strictly constant at finite temperature. Similar to the variations in the on-site energies discussed in section 3.3, the variations of the intermolecular couplings are also of importance, that is, slow dynamic disorder at room temperature influences these quantities as well,[124] as variation of the transfer integrals can reach the same order of magnitude as the average values.[85] **Figure 9** illustrates these dynamic fluctuations for the case of HOMO transfer integrals in pentacene for various molecular pairs.

To account for such fluctuations, the second extension of the purely electronic Hamiltonian description beyond single-molecular properties (after including the ε_{MN}) therefore concerns the non-local coupling to phonons, $g_{MN\lambda}$, that is, the changes in the transfer integrals due to vibrations. From simple considerations, it is clear that the non-local electron–phonon coupling is becoming more important in systems where the electron transfer integrals are small as we illustrate in the next section. In addition, as a trend one finds that transport mediated by non-local electron–phonon terms increases in importance at higher temperature.[125]

Experimentally it is much more difficult to access non-local couplings than local ones, as they are related to intermolecular vibrational modes, which cannot be resolved currently in ARPES or related techniques. We therefore rely on first-principles simulations of crystal band structures and their phonon-induced modifications to obtain quantitative values to determine this part of the Hamiltonian. With such values and corresponding theory, however, it is possible to understand experimental evidence of non-local electron–phonon couplings as well, as will be discussed below.

4.2.2. Experimental Observation for Naphthalene

Here we would like to discuss the influence of non-local electron–phonon interaction on the electron transport in naphthalene single crystals. As mentioned above the herringbone stacking implies a small transfer integral in the out-of-plane direction. For naphthalene this is the c'-direction. Time-of-flight measurements of the electron mobilities[119,126] show a steep decrease with temperature between 4 K and 100 K, followed by a remarkable temperature independent mobility between 100 K and 300 K along c' (see **Figure 10**).

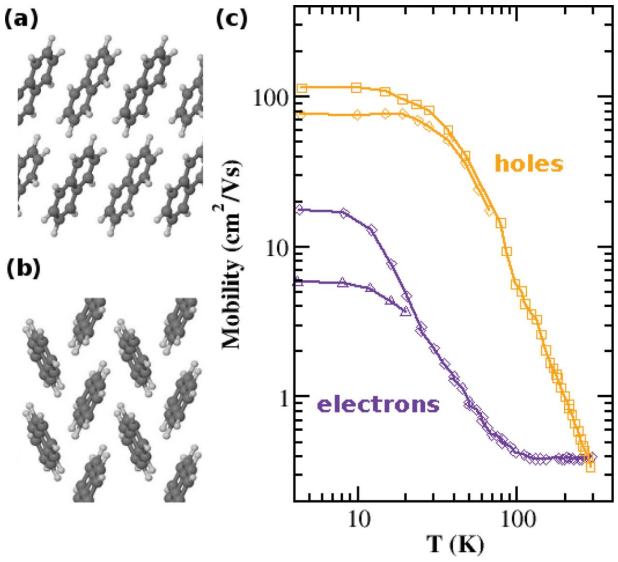

Figure 10. a,b) Crystal structure of naphthalene. a) View in *b*-direction exhibits vertical stacking of herringbone planes (c' points upwards). b) View along c'- direction (monoclinic *b* axis upwards) shows a 2D herringbone stacking of molecules in planes. c) Hole and electron transport in c' (out-of-plane) direction in naphthalene crystals taken from the literature.[126] Different symbols indicate different electric fields.

This characteristic behavior is currently understood[127] as a result of an interplay of band transport at low *T*, which stems from the electron transfer integral in *c*-direction ε_c' and phonon-assisted hopping at elevated *T*, which arises from the sizeable non-local coupling in *c*-direction. Taking a closer look at the parameters, it is clear that due to the small ε_c (which is about one order of magnitude smaller than transfer integrals within the herring-bone plane,[125] band transport can hardly be observed at room temperature. On the other hand, the significant non-local electron–phonon coupling g_c triggers strong phonon-mediated conduction, which leads to a departure of the characteristic low-*T* power-law temperature dependence and the observed remarkable mobility saturation.[127] In contrast to electrons, the hole transfer integral in the same transport direction is much larger, resulting in power-law behavior of the mobility up to room temperature and a weak influence of the corresponding electron–phonon coupling g_c for holes.

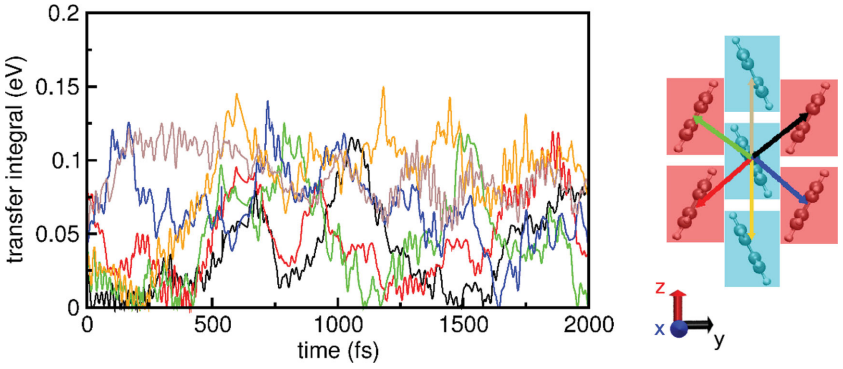

Figure 9. a) Time dependent variations of nearest-neighbor transfer integrals in pentacene and b) corresponding pair of molecules in the pentacene crystal.

4.3. Charge Transport Approaches in Bulk Materials

4.3.1. Electron Transfer Theory

In order to start with a conceptually simple approach, we describe briefly the related

elementary problem of a charge transfer process (an elementary hopping process) between a donor-acceptor pair according DA->D^+A^-. Such processes are ubiquitous in biology and chemistry and their understanding is central to many important phenomena. One can imagine that consecutive hops occur also in bulk transport (where A and D may be of the same species), which is indeed what can be derived in a certain limit of a more general approach.

Electron transfer theory was initially worked out via classical electrostatic considerations by R. A. Marcus,[128] where fluctuations in the surrounding of the donor and acceptor species trigger the charge transfer process via activated states. A quantum theory was put forward by Levich[129] and Jortner,[130] while the seminal papers of Holstein[83,84] had described previously analogous effects in solids. The derived formalisms are based on the understanding that non-adiabatic processes are involved in the charge transfer problem, since transfer integrals are small. One of such formulations is based on Fermi's golden rule, which treats the transfer integral between the species as a small perturbation and results in the following transition rate between molecules *M* and *N*:

$$\nu_{MN} = \frac{1}{\hbar}|\varepsilon_{MN}|^2 \exp\left[-\sum_{\lambda}(1+2N_\lambda)g_\lambda^2\right] \int_{-\infty}^{\infty} \mathrm{d}t \exp\left[i(\varepsilon_M - \varepsilon_N)t/\hbar\right] \exp\left[2\sum_{\lambda}\phi_\lambda g_\lambda^2\right] \quad (21)$$

where $\phi_\lambda(t) = N_\lambda e^{i\omega_\lambda t} + (N_\lambda + 1)e^{-i\omega_\lambda t}$ and N_λ is the number of phonons following the Bose-Einstein statistics. In the above equation g_λ represents the local electron–phonon coupling constant for mode λ, that is, non-local terms are not considered at the moment. From this transition rate one calculates the mobility according to $\mu = \frac{\nu_{MN} R_{MN}^2 e_0}{k_B T}$, where the hopping distance in transport direction R_{MN} between sites *M* and *N* has been introduced.

It is instructive to briefly discuss the influence of the material parameters and the involved processes. First, in the limit of zero electron–phonon coupling, the transfer rate is determined by the electronic energy scale ε_{MN} through its squared modulus in the prefactor. This prefactor (together with R_{MN}^2 can impose transport anisotropy, which is frequently observed in experiments on crystalline structures.

In molecular materials, finite g_λ impose an additional constraint for the transfer process arising from the nuclear subsystem and leading to an exponential reduction of the rate ν (first exponential in Equation 21) due to geometrical relaxation effects upon charging. Different names have been coined for this in different contexts, such as polaron band narrowing, Debye-Waller factor, or Franck-Condon factor. Second, direct and indirect transitions ($M \rightarrow N$) are allowed where a possible energy difference between the involved states can be compensated by phonons, for example, $\varepsilon_M - \varepsilon_N = \hbar\omega$ in a single phonon absorption/emission event or by any combination of involved phonon frequencies in higher-order phonon absorption and emission processes (encoded in $\phi_\lambda(t)$). Note that the importance of the electron–phonon coupling lies in the intermixing of such phonon-mediated charge transfer processes into the fully coherent transport contributions. Finally, the subtle interplay between band narrowing effects and phonon-assisted transport enhancement strongly depends on the size of the coupling constants governing the amount of phonon-assisted transport contributions.

It is clear that the expression derived within Fermi's Golden Rule is valid if the initial and final states have very long lifetimes, which has to be checked carefully. In view of the non-vanishing values of transfer integrals and their oscillations (cf. Figure 9) this might seem questionable. In fact, this is one of the most difficult tasks to do for the general situation in organic matter, as it depends on many factors, not only on the transfer integrals ε_{MN}, but also on the couplings g_λ as well as on disorder, temperature, carrier concentration, and electric fields. Therefore, too simplified approaches are relatively limited in adding to our understanding of transport in organic materials.

4.3.2. Polaron Transport Theory

An extension beyond the Fermi Golden Rule is possible in the polaron treatment, which allows extending the applicability to finite transfer integrals. Such approaches can be hosted in the general framework of Kubo's linear response theory[131] relating the current through a system to the applied electric field via the conductivity

$$\sigma_{\alpha\beta} = \frac{1}{2k_B T}\lim_{\omega\to 0}\int_{-\infty}^{\infty}\mathrm{d}t e^{i\omega t}\left\langle j_\alpha(t)\, j_\beta(0)\right\rangle_H \quad (22)$$

where the current operators are defined as $j = \frac{1}{i\hbar}[P_\alpha, H]$ with the polarization $P_\alpha = e_0\sum_M R_M a_M^\dagger a_M$ and the operator average $A_H = \mathrm{Tr}\left[e^{-H/k_BT}A\right]/\mathrm{Tr}\left[e^{-H/k_BT}\right]$. The Cartesian indices (α,β) indicate the tensor character, which can often be simplified to diagonal contributions, that is, electric field and current are aligned ($\alpha = \beta$). Besides taking electrons and phonons as basic variables, one can better describe the phonon dressing of the charge carriers in an alternative treatment which uses composite particles (quasiparticles) consisting of the charge and its polarization cloud as a new entity through a unitary Lang-Firsov transformation. One writes

$$\sigma_{\alpha\alpha} = \frac{1}{2k_B T}\int_{-\infty}^{\infty}\mathrm{d}t\left\langle \tilde{j}_\alpha(t)\,\tilde{j}_\alpha(0)\right\rangle_{\tilde{H}} \quad (23)$$

The evaluation of the correlation function of polaron-current operators $\tilde{j}$ is a difficult task. For the limit of very small electronic transfer integrals this problem is strongly simplified and for crystalline structures it can be expressed as

$$\sigma_{\alpha\alpha} = \frac{e_0^2 c(1-c)}{2k_B T\hbar^2}\sum_M R_M^2\tilde{\varepsilon}_{0M}^2\int_{-\infty}^{\infty}\mathrm{d}t\,\exp\left[2\sum_\lambda\phi_\lambda(t)g_\lambda^2\right]e^{-t^2/\tau^2} \quad (24)$$

Again the Franck-Condon factor appears in the polaron transfer integrals $\tilde{\varepsilon}_{0M} = \varepsilon_{0M}\exp\left[-\frac{1}{2}\sum_\lambda(1+2N_\lambda)g_\lambda^2\right]$ introduced here. While this formula does not explicitly treat different

on-site energies and transfer integrals, disorder effects can be described with the empirical parameter τ. If we continue with the calculation of the carrier mobility $\mu = \frac{\sigma}{e_0 c}$, one recognizes that the expression for the mobility is at the same level of description as Fermi's Golden Rule, that is, it is perturbative in the transfer integrals ε_{0M}, and we have merely obtained the same result in a different way.

However, an extension of this approach over a perturbative treatment of the transfer integral, which leads to a significant improvement of the qualitative description of carrier transport, is possible when (although assuming polaron dressing) a finite polaronic bandwidth is still taken into account.[132] One can derive the following expression

$$\mu_{\alpha\beta} = -\frac{e_0}{2N_C N_\Omega \hbar^2 k_B T} \sum_{LMN} R_{L\alpha} R_{N\beta} \tilde{\varepsilon}_{0L} \tilde{\varepsilon}_{0N} \sum_{\mathbf{k}_1 \mathbf{k}_2} e^{-i\mathbf{k}_1(\mathbf{R}_M + \mathbf{R}_N)} e^{i\mathbf{k}_2(\mathbf{R}_M - \mathbf{R}_L)} n_{\mathbf{k}_1}(1 - n_{\mathbf{k}_2}) \int_{-\infty}^{+\infty} \mathrm{d}t e^{\frac{it}{\hbar}[\tilde{\varepsilon}(\mathbf{k}_1) - \tilde{\varepsilon}(\mathbf{k}_2)]} \exp\left\{-\sum_{\mathbf{Q}} \phi_Q(t) G^Q_{0L0N} e^{-i\mathbf{Q}\mathbf{R}_M}\right\} \quad (25)$$

The finite bandwidth is reflected in the Fermi function for polarons $n_{\mathbf{k}_1} \equiv n_{\tilde{\varepsilon}(\mathbf{k}_1)}$, which goes beyond the prior assumption of a constant occupation number c in Equation 24. For completeness, we mention that the mode index Q in the above expression includes phonon branch and wave vector q for phonons and the quantity $G^Q_{0L0N} = \left(g_{Q00} - g_{QLL}\right)\left(g_{Q00} - g_{QNN}\right)$ is related to the squared coupling constants which appeared in the perturbative result (Equation 24) in a simpler form.

The evaluation of Equation 25 assumes the knowledge of all material parameters such as molecular geometry, transfer integrals, phonon frequencies, and electron–phonon couplings. It is more elaborate than Equation 21, since more sums have to be performed and more terms calculated. For convenience, however, it can be split into two distinct terms. One term describes coherent band transport and can be obtained by setting $G^Q_{0L0N} = 0$ in Equation 25, which then can be expressed as

$$\mu^{(\mathrm{coh})}_{\alpha\beta} = \frac{\sqrt{\pi} e_0}{2N_C k_B T} \sum_{\mathbf{k}} n_{\mathbf{k}}(1 - n_{\mathbf{k}}) \tilde{v}_\alpha(\mathbf{k}) \tilde{v}_\beta(\mathbf{k}) \tau(\mathbf{k}) \quad (26)$$

In fact a similar expression is well known from Boltzmann equation-based transport simulations, where the relaxation time τ is calculated perturbatively.[133] Here it appears in its phonon-dressed (polaron) version, where $\tilde{v}_\alpha$ is the polaron band velocity. For a detailed discussion of the remaining phonon-assisted transport terms μ–$\mu^{(\mathrm{coh})}$ we refer to another study.[132] Here we only mention that both contributions have varying influence in dependence of temperature and disorder as well as material parameters.

Before we discuss the effect of disorder in more detail in the next section we note that the expression 25 is still to be extended to describe non-local electron–phonon coupling which is presently not included. The discussions in Section 4.2. and in the literature[127] indicate the conditions where changes in the transport behavior compared to Equation 25 can be expected, namely when very small transfer integrals and large non-local electron–phonon couplings occur in one direction.

5. Modelling Disordered Organic Systems

5.1. General Considerations

As organic semiconductors are appearing in single crystalline phases and more or less disordered phases with varying morphologies, it is useful to extend the above approaches to disordered systems. Clearly the phenomenological parameter τ, an effective scattering time, has to be replaced by a microscopic model of disorder scattering to get an understanding of the influence of disorder. Below, we show how this can be achieved by simultaneously keeping a high level of theoretical description and specificity through using the full set of ab initio material parameters.

On the other hand, if such material-specific information is not available or disorder dominates, one may recourse to simpler approaches. As an extreme limit one may assume situations where disorder exclusively determines transport properties without any remaining trace of the specific material. We first focus on the former case by extending Equation 25 to situations of weak disorder. Strongly disordered materials are described briefly afterwards for completeness.

5.2. Weak and Medium Disorder

For the coherent part of transport processes, that is, where phonon-assisted contributions are insignificant, one can rephrase Equation 26 in real space, where it is directly related to the diffusion coefficient

$$D(E) = \frac{\mathrm{d}}{\mathrm{d}t} \mathrm{Tr}\left[\delta\left(E - \tilde{H}\right) \Delta X^2(t)\right] / \mathrm{Tr}\left[\delta\left(E - \tilde{H}\right)\right] \quad (27)$$

which describes the mean square displacement of coherently propagating wave packets $\Delta X^2(t) = \left[x(t) - x(0)\right]^2$ at a given energy E. Equation 27 goes beyond Equation 26 in that one can model generally disordered systems where various scenarios for morphologies can be described. The diffusion coefficient $D(E)$ is further related to the conductivity via

$$\sigma(E,t) = e_0^2 \rho(E) D(E) / 2 \quad (28)$$

where $\rho(E) = \mathrm{Tr}\left[\delta\left(E - \tilde{H}\right)\right]$ is the density of states of the disordered system. From this, the temperature-dependent coherent mobility (introducing a coherence time τ_c) can be obtained as[134]

$$\mu^{(\mathrm{coh})} = \frac{\Omega}{e_0 c k_B T} \int \mathrm{d}E n(E)\left[n(E) - 1\right] \sigma(E, \tau_c) \quad (29)$$

Using the polaron Hamiltonian $\tilde{H}$ in Equation 27–29 along with microscopic disorder terms is a way to generalize Equation 26 beyond a simple relaxation time approach. One should keep in mind that the coherent mobility Equation 29 represents only one part of all transport contributions. The remaining phonon-assisted transport terms have been derived elsewhere[134] and will not be discussed in detail. Rather, with these two contributions at hand, we show an illustration of the influence of disorder on the carrier mobility. For simplicity, we have carried out these simulations on a level of model calculations with pure on-site disorder,[134] where the on-site energies are random variables chosen from a given interval $[-W/2,W/2]$ and W defines the disorder strength.

Figure 11 shows carrier mobilities in a model of an organic crystal with their full temperature dependence. We find that the temperature dependence is clearly affected by changes in the strength of disorder. For small values of the on-site disorder (W = 40 meV corresponds to a standard deviation of 10 meV) there is clear band-like transport with decreasing mobilities for increasing T. When increasing W, the mobility drops strongly at low temperature leading to a strong trapping behavior at even larger disorder (W = 160 meV). The effect is also observable at room temperature though much less strongly. A more refined disorder potential, including off-diagonal disorder should lead to a further improvement of the qualitative and quantitative description of realistic traps which may also be characterized by correlations in the on-site energies beyond the model discussed here. Also a study with lower carrier concentrations would be desirable to analyze trapping and de-trapping behavior in more detail.

Figure 11(c) shows the total mobility, which is a sum of the coherent and incoherent contributions. Incoherent contributions occur for temperatures above 100 K. This is an interesting regime as molecular and/or lattice vibrations are directly involved and assist transport. Still between 100 K and 300 K the mobility drops which is mainly driven by the phonon-assisted terms in the total mobility. This behavior may appear puzzling at first sight but can be rationalized as follows. Although the phonons do assist the carrier transport and are necessary for this contribution to be non-vanishing, the temperature dependence, that is, the mobility decay with increasing T (and increasing number of phonons), is attributed to the scattering by phonons. Such scattering and promoting nature of phonons shows their ambivalent role in the transport problem of molecular semiconductors.

The aspect of scattering of charge carriers by phonons can be captured by the concept of dynamic disorder which is used frequently in literature based upon a semiclassical approach. Indeed similar temperature dependence to the one observed in Figure 11c can be captured in approaches based on simulating the electron quantum dynamics under time-dependent potentials.[135–138] In such approaches, the phonons are not included as quantum objects but described as classical subsystem which can couple to the electrons in a time dependent fashion, where for the technical treatment different ways have been proposed. Dynamic disorder can therefore be regarded as semiclassical analog to the phonon-assisted transport described above, while the notion itself disregards the activation aspect although it is also part of these formalisms.

Finally, static disorder is readily included in such approaches while several other extensions are still to be worked out and deserve further attention in the future.

5.3. Approaches for Disorder-Dominated Systems

When considering the limit of very strong disorder, the energy scale of disorder will dominate the characteristic energies associated to the organic material (transfer integrals, etc.). In such cases generic approaches can be used to model transport, which no longer take material specific parameters into account. Among them we mention Monte Carlo-based semi-classical hopping models,[139] which can be based on a Miller-Abrahams hopping rates[140]

$$\nu_{MN} = \nu_0 \exp\left[-2\gamma R_{MN}\right] \begin{cases} \exp\left[-\dfrac{\varepsilon_N - \varepsilon_M}{k_B T}\right], & \varepsilon_N > \varepsilon_M \\ 1, & \varepsilon_N < \varepsilon_M \end{cases} \tag{30}$$

Such schemes can be run for sets of on-site energy distributions (e.g., assuming Gaussian distribution with standard deviation σ) and the results can be compared to the measured transport data to extract an effective disorder strength σ_{eff} and other empirical parameters which can be interpreted as a maximum hopping rate (ν_0) and an effective overlap coefficient (γ_{eff}). This approach can be useful to characterize

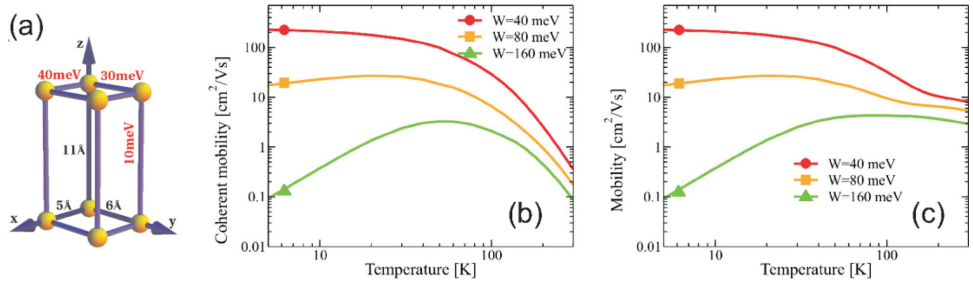

Figure 11. Simulations on the influence of disorder on carrier transport in a model crystal subject to disorder. a) Definition of material parameters representative for an organic crystal. A single mode with energy $\hbar\omega$ = 12 meV and effective electron–phonon coupling of $g = 0.7$ was assumed. Carrier density $N_c/N_\Omega = 10^{-3}$. b) Coherent transport simulations with Equation 32. c) Carrier mobility including coherent transport and incoherent hopping motion. Adapted according to Ref. [134], with permission. Copyright 2011 American Physical Society.

different morphologies when only little further information is available.

If, in contrast, the system is better known and some material parameters can be obtained, one can also use the hopping rates (21) along with Monte Carlo schemes. Ultimately however, one is interested in maximizing predictability based on transport simulations which requires to obtain both the best theoretical model and material parameters on the most accurate level.

6. Determination of Material Parameters

6.1. First-Principles Calculations

An important task for the simulation of organic semiconductors is the description of their electronic structure as well as their vibrational properties. State-of-the-art first principles simulations are capable of describing several hundreds of atoms and unit cells of 1–2 nm size. While this is sufficient to simulate small systems (molecules or metallic wires) in-between metallic electrodes[141,142] and organic–inorganic interfaces[143] for example, larger devices generally evade such first-principles description simply because of their size. It is therefore appropriate to recourse to finite-sized tight-binding Hamiltonians, as introduced in the above sections to describe relevant interactions and to identify the electronic parameters in such Hamiltonians with the corresponding material parameters of the compound under study. Still such material parameters have to be determined by first principles calculations. However, this can be carried out for single molecules or smaller clusters of molecules, which strongly reduces the necessary size of the system and is treatable on the first-principles level.

There is a large variety of different approaches for electronic structure calculations. Besides standard density functional theory (DFT),[144] which is an exact theory for ground state properties, there exist several quantum-chemistry approaches capable of accurately describing the electronic structure. In DFT many density functionals have been developed in the past decades each of which has its own characteristics. The local density approximation (LDA),[145] the generalized gradient approximation (GGA),[146] or different van der Waals-corrected GGA flavours (GGA+vdW)[147–149] as well as hybrid functionals[150] form the largest families. While a detailed assessment of those methods is not within the scope of the present paper, a balance between computational cost and accuracy is desirable while systematic improvements in accuracy are possible.

6.2. Single-Molecular Properties

On the molecular level, one routinely obtains charging energies of the molecules (electron affinity and ionization potential) as well as spectroscopic quantities and vibrational properties. In particular, the latter can be obtained from a series of total energy calculations with atomic displacements from the geometric ground state. The on-site energy, that is, the energetic position of the frontier orbitals (HOMO or LUMO) that are relevant for electron and hole transport (described at a sufficiently high level of theory), can be expressed as $\varepsilon_M = \langle \psi_M | \hat{H}_{\text{eff}} | \psi_M \rangle$, where $\langle | \psi_M \rangle$ is a frontier orbital.

Local electron–phonon coupling parameters are calculated when vibrational distortions are imposed onto the molecule. A frozen phonon calculation with the phonon mode λ may lead to a change in ε_M, which by a linear fit with respect to the displacement directly gives the local electron–phonon couplings through Equation 16. Comparisons of values obtained from different first-principles approaches in case of C_{60} can be found in the literature.[151]

6.3. Molecular Aggregates

For condensed-phase structures (molecular crystals or clusters) the electronic coupling between adjacent molecules entails finite transfer integrals, which can be written as

$$\varepsilon_{MN} = \langle \psi_M | \hat{H}_{\text{eff}} | \psi_N \rangle \tag{31}$$

Together with the on-site energies, this describes the electronic properties in the Hamiltonian. When using gas-phase molecular orbitals for the calculation of ε_{MN}, one has to remember, however, that these orbitals also have a finite overlap $S_{MN} = \langle \psi_M | \psi_N \rangle$, that is, they are not orthogonal. Orthogonal basis states, however, are usually assumed in theoretical derivations, such as the ones displayed above, as this is much easier to use. A solution to this problem is to orthogonalize the basis after performing the DFT simulation by means of Löwdin's symmetric transformation[152] while maintaining as much as possible of the initial local character of the frontier orbitals:

$$(\varepsilon')_{MN} \approx \varepsilon_{MN} - \frac{1}{2} S_{MN} (\varepsilon_{MM} + \varepsilon_{NN}) \tag{32}$$

For the calculation of the non-local coupling as present in Hamiltonian 20, the variation of the transfer integrals due to vibrations (fluctuation of the spacing between molecules and/or the relative orientations of adjacent molecules) are obtained for a displaced geometry as in the local case such that one obtains $g^{\mathbf{Q}}_{MN}$ from linear fits as the non-local version of Equation 16.

At this point, one should mention that non-local parameters ε_{MN} and $g^{\mathbf{Q}}_{MN}$ may depend not only on the two considered sites (or molecules) M and N but, as molecular packing is dense, closely adjacent molecules may also have to be considered during the simulation. This requires performing DFT simulations for trimers, tetramers or eventually even larger assemblies, which increases the computational effort.

6.4. Crystals

For molecular crystals one naturally uses electronic band structure calculations in order to obtain a set of electronic parameters. Including as a first step the on-site energies and nearest neighbors as parameters, one can set up a Bloch Hamiltonian with the dimension of the number of orbitals per unit cell. Most often one finds two molecules per unit cell, which yields a 2×2 matrix for each wave vector k. By

diagonalization, the two bands are analytically obtained and the expressions $(\varepsilon')_{\mathbf{k}} = \pi_{\mathbf{k}} \pm \sqrt{\sigma_{\mathbf{k}}}$ can be fitted to the ab initio band structure (e.g., by a least squares fit on a regular grid in the Brillouin zone). During the fit procedure, one takes into account the symmetry of the crystal, which reduces the number of independent parameters. In this way, the ab initio band structure is mapped onto a set of parameters that are effective transfer integrals (ε_a, ε_b, ε_c, etc. for lattice directions and $\varepsilon_{\pm\frac{a}{2}\pm\frac{b}{2}}$ and similar terms for diagonal directions) and orthogonalization is not necessary. The accuracy of the fit can be improved systematically upon extending the set of neighbors.

An analogous procedure is carried out for the extraction of the electron–phonon coupling constants. Here, the ground state electronic structure obtained in the first step and the corresponding set of transfer integrals serve as reference to measure changes in the band structure that are induced by phonon modes. These changes in the band structure ($\Delta\varepsilon_a$, $\Delta\varepsilon_b$, $\Delta\varepsilon_c$, $\Delta\varepsilon_{\pm\frac{a}{2}\pm\frac{b}{2}}$, etc.) yield the non-local couplings analogous to Equation 16.

7. Open Challenges and Perspectives for Experiment and Theory

7.1. Experimental Challenges and Open Questions

Research on OFETs started more than 25 years ago[153–155] and has made tremendous progress in terms of performance and understanding over these years. But despite the massive research in the last decade, OFET-enabled products have not yet entered the mass market. Organic electronics are anticipated to open the route to low-cost, flexible electronics. Their applications range from disposable radio frequency identification (RFID) tags and microprocessors to the driving transistors of displays – each of them requiring specific device parameters.

The realization of efficient complementary logic, for example, requires p- and n-type OFETs. While current p-type organic transistors meet the requirements here, typical n-type devices still exhibit lower current densities, transit frequencies, as well as stability. Furthermore, the transit frequency has to be further improved for the application in RFID tags. First microprocessors have been realized, operating at a frequency of up to 70 Hz.[21] RFID tags, however, typically operate at a frequency of 13.56 MHz. Even though required transit frequencies should be feasible,[156] these operation frequencies are far from standard in current flexible devices. The application as driving transistors in flexible displays, in turn, will benefit from an increase of on-state current. Even though current OFET devices can supply the current necessary to drive an OLED pixel, for example, a higher on-state current enables smaller footprint and therefore a better fill factor in the final display. All these parameters can be addressed by the material design, for example, an improvement in stability and charge carrier mobility, and the scaling of the characteristic device dimensions. One promising approach to further improve organic transistors are vertical approaches, which can deliver very high current densities.[157]

7.2. n-Type Devices

While it is possible to realize inverters and more complex logic functions with only one type of transistor, complementary circuits offer higher noise immunity as well as lower static power consumption. In contrast to inorganics, however, n-type operation faces a few challenges in organic electronics. The injection of holes into the HOMO level of the semiconductor for p-type operation is easily achieved using Au electrodes, as many of the typical organic semiconductors have an ionization potential (IP) in the range of 5 eV. With this alignment, however, the barrier for injecting electrons into the LUMO of the materials is as large as 2–3 eV. Consequently, n-type operation was initially only observed in devices employing low work function metals (e.g., Ca) as electrodes.[158] A shift of the IP to values above 4 eV[159] makes n-type operation possible with air-stable electrodes, however, inert atmosphere is still needed during operation, as the radical organic anions generated close to the gate dielectric are typically unstable towards reduction of water or oxygen diffusing into the semiconductor layer.[160]

Besides encapsulation and a hydrophobic gate dielectric, a close packing of the molecules seems to be beneficial for reducing the diffusion of water into the channel region.[158,161] Even though a mobility of up to 1.3 cm^2/Vs was demonstrated in air-stable n-type OFETs,[162–164] a further improvement of the mobility is necessary for a successful integration into more complex devices.

Additionally, interface states at the semiconductor/dielectric interface play a crucial role for the operation of n-type OFETs. Many inorganic gate dielectrics tend to offer efficient electron traps. The widely used SiO_2, for example, has a large number of OH-groups capable of electron trapping. Consequently, many organic semiconductors previously exhibiting only p-type transport are capable of n-type operation on hydroxyl-free gate dielectrics.[165,166] Hence, a detailed understanding of the semiconductor/dielectric interface is essential to successfully model the device characteristics.

7.3. Scaling of the Characteristic Device Dimensions

Transistor performance, and OFET performance in particular, is highly dependent on device geometry. Aggressive scaling of the relevant device dimensions can therefore lead to significant improvements in OFET performance, while equally providing a better understanding of the functional principles of the device in question. One approach to realize such aggressive scaling is the use of high-*k* dielectrics or self-assembled monolayers as OFET gate dielectric[167–169] in order to enhance the field-effect produced by the gate electrode and decrease the hysteresis and bias-stress effects often present for SiO_2-based dielectrics.[169,170]

As can be seen from Equation 4,5, the MOSFET formalism further suggests an increase of output current I_D with decreasing channel length L, as is also true for the OFET's cut-off frequency, which scales as $f_T \propto \frac{1}{L^2}$.[156] Additionally, the poor charge transport in organic semiconductors, especially across grain boundaries of amorphous or polycrystalline materials, favors short conduction paths. Drastically reducing the transistor channel length is therefore one of the main issues in

current OFET research and has been attempted several times over the years.[156,167,171] Reduction of the channel length beyond a critical point (which depends on the device in question) always leads to so-called short channel behavior[156,171–174] and an increasing limitation of the OFET performance by contact resistance.[156,168,175–177] While the study of this short channel behavior can lead to a better understanding of the underlying device and transport physics, it is often difficult to realize such short channel devices experimentally, especially for top contact devices, as high-resolution patterning techniques need to be employed on top of the organic semiconductor in this case to structure the OFET electrodes. Furthermore, the contacts in such devices are often doped in order to enhance charge carrier injection and thus reduce the influence of contact resistance,[168,178–183] a method which becomes increasingly difficult at short channel lengths due to diffusion of the dopant into the conductive channel.

7.4. Materials and Morphology

Besides the dimensions of transistor devices, the mobility of the organic semiconductor is the main limiting factor for the overall device performance. The on-state current (Equation 4,5) as well as the transit frequency are directly proportional to the charge carrier mobility.[156] Consequently, a great measure of the progression in recent years relates to an improvement of mobility. As described in the previous paragraphs, the charge carrier transport in weakly interacting organic semiconductors is determined by the transfer integral between neighboring molecules as well as the trap density. The trap density is mostly addressed by increasing the material purity in the experiment. With vacuum sublimation for small molecules and the synthesis of polymers based on highly purified monomers, high purity organic semiconductors are readily available.

For an efficient charge transfer between neighboring molecules, a large overlap of the frontier orbitals is important. This overlap depends, on the one hand, on the extension of the corresponding delocalized orbitals (HOMO for hole and LUMO for electron transport) and can be different for electrons and holes.[90] Furthermore, the reorganization energy of the molecules depends on the molecular structure. Hence, a proper material design results in potentially high charge carrier mobilities. On the other hand, to ensure an efficient overlap, the molecular packing has to be adjusted accordingly. While amorphous organic semiconductors with a random orientation of neighboring molecules typically only exhibit mobilities in the range of 10^{-6} to 10^{-3} cm^2/Vs, the highest charge carrier mobilities for thin films have been observed in highly ordered polycrystalline layers[54,55] with the highest molecular order provided in single crystals.[56,57] The crystalline growth, in turn, leads to an anisotropic charge carrier mobility. Consequently, a beneficial orientation of the high mobility direction parallel to the channel has to be ensured in transistor design.

A deliberate modification of the semiconductor/dielectric interface, e.g., by treatment with a self assembled monolayer, addresses several issues at once. While it can reduce the trap density at the interface,[170,184,185] the surface energy of the interface modifies the crystallite size and orientation within the channel.[186,187] Pentacene, for example, exhibits a partial overlap of the HOMO of neighboring molecules in the (001) plane of the pentacene crystal and favorably grows with this axis parallel to the gate dielectric.[53,186,188] The high crystallinity, resulting in high mobility, however, simultaneously leads to a lower reproducibility of device parameters. While the increase of crystallite size yields the desired increase of charge carrier mobility, the disturbing effect of grain boundaries becomes more important. Consequently, the devices recently demonstrating record mobilities suffer from a large sample-to-sample variation.[54,55] Furthermore, the stability of device parameters in flexible devices—one of the anticipated applications of organic electronics—is affected by an increasing effect of grain boundaries.[189]

Finally, the challenges described here ultimately impact the agreement between experiment and theory. The strong dependency of the charge carrier mobility on the molecular arrangement as well as the trap density renders the prediction of the device performance based on a purely microscopic theory of transport difficult. While the crystal structure as well as the average crystallite size can be precisely determined by experimental methods, the molecular arrangement at grain boundaries cannot be easily extracted. A theoretical description of the devices with an average transfer integral works for amorphous or purely crystalline semiconductors. As grain boundaries start to dominate the device performance for efficient polycrystalline devices, a detailed knowledge of structure as well as transport across these boundaries is crucial. The same holds true for the effects at the semiconductor/dielectric interface, where the contribution to the device performance has to be analyzed thoroughly in experiment, as well as in theory.

An alternative approach to improve OFET performance for commercial applications must therefore be the design of new device concepts, such as the organic JFET,[190] inversion OFETs,[191] and vertical OFETs.[192–196] For the latter case in particular, the functional principles are as yet unclear and extensive simulations are needed in order to understand the underlying physics of these vertical devices in more detail.

7.5. Microscopic Theory of Charge Transport

From the theoretical point of view it is very challenging to provide the field with sophisticated models, tools, and concepts to describe charge-carrier transport in a rather general approach because, as mentioned in the introduction, there are many characteristic energies involved in this description which are similar in size (such as transfer integrals, thermal energy, phonon frequency, polaron binding energy, and disorder). The role of each of these—taken alone—is rather evident, however, their interplay is not.

It is therefore very helpful when some of these effects can be neglected under certain conditions, for instance, at low temperature, in ultrahigh vacuum conditions or in single molecule experiments, which reduces complexity. However, even there many theoretical questions are unanswered, such as the precise role of polaronic relaxation for transport if the transport time between electrodes is very long.[197]

On the other hand, reducing complexity is desirable when addressing fundamental questions. When it comes to

applications, however, full functionality of the materials and systems is key, regardless of their level of understanding. Still we believe that application-driven questions and fundamental questions are closely connected by the concept of rational design which ultimately depends on the ability to predict properties of new molecular materials and therefore on their full understanding at all involved length scales from the intramolecular bonds to the device scale.

Evidently this requires the combination of several tools. First, ab initio simulations are essential where, despite of its known shortcomings, DFT is a highly successful framework to describe materials from bulk systems to nanostructures. The prediction of molecular properties including their optoelectronic characteristics is one of the success stories of quantum chemistry although there is room for improvement in terms of accuracy and speed of the simulation algorithms.

Second, for the connection to a larger length scale (the mesoscopic scale) of devices, material parameters obtained from DFT are basic ingredients, entering trough the definition of the system Hamiltonian. These parameters are not yet automatically obtained in DFT codes, but require interaction with the researcher, which is a severe bottleneck. This is only partly due to insufficient accuracy of DFT methods.

Additionally, when aiming for a microscopic picture, there is the inevitable question of the underlying supramolecular structure. Its prediction is not only a challenge for theory, but also in experiment the microstructure is often not fully clear.[198] If sufficient information about microstructure were available and microscopic material parameters be calculated, multiscale-type simulations could be carried out taking into account additional external parameters such as temperature, electric field distributions etc.

Finally, once the material parameters are known, the choice of transport approach is to be made, where analytical, numerical, and mixed approaches are available on different stages of development. In general, semiclassical approaches can capture the high-temperature regime but have no access to quantum-tunneling effects.[199,200] On the other hand, time-propagation methods and analytical approaches have to be improved and/or extended to be comparable in the future which remains an important task to improve our basic understanding.

8. Summary and Conclusion

We have tried to give an overview over several ways to study and exploit molecular materials as electronic components in various devices. We have illustrated concepts and theoretical frameworks adapted to the specific situation encountered in single-molecule and supramolecular transport experiments. Thereby we focused on a particular feature of molecular materials, the importance of electron–phonon coupling, which manifests in many effects from inelastic tunneling and optical spectroscopy to the transport regime in bulk organic semiconductors.

The selection of topics that we were focusing on entailed that we could not include other important topics in organic materials such as interface effects or exciton physics and energy transfer. Also we have disregarded other interesting applications beyond charge transport (such as thermoelectrics, magnetotransport or spin effects).

Finally we have attempted an outlook for possible future development and needs for further progressing the field of organic electronics. Both theoretical and experimental challenges demand for strong efforts, which in future should ideally be aligned and ultimately be guided by efficient and successful rational design.

Acknowledgements

This work is partly based on original research of H. Kleemann, D. Nozaki, and K. Hannewald. The authors gratefully acknowledge fruitful discussions with all of them. F.O. would like to thank the DFG for financial support within the Emmy-Noether funding scheme and A.G. thanks the Dr. Isolde-Dietrich-Stiftung for its financial support. This work was partly supported by the DFG within the Cluster of Excellence "Center for Advancing Electronics Dresden". The authors acknowledge the Center for Information Services and High Performance Computing (ZIH) at TU Dresden for computational resources.
Note: the layout of Equation 30 was changed after initial online publication to make it clearer. The content of the equation was not altered. The change was implemented on April 1, 2015.

Received: July 14, 2014
Revised: September 11, 2014
Published online: October 14, 2014

[1] E. A. Silinsh, V. Capek, *Organic Molecular Crystals*, American Institute of Physics, New York, USA **1994**.
[2] We mention explicitly the counterexample of polymerization from oligomer precursors on surfaces, which is an interesting field by itself.[3]
[3] J. Cai, P. Ruffieux, R. Jaafar, M. Bieri, T. Braun, S. Blankenburg, M. Muoth, A. P. Seitsonen, M. Saleh, X. Feng, K. Müllen, R. Fasel, *Nature* **2010**, *466*, 470.
[4] M. Granström, K. Petritsch, A. C. Arias, A. Lux, M. R. Andersson, R. H. Friend, *Nature* **1998**, *395*, 257.
[5] S. E. Shaheen, C. J. Brabec, N. S. Sariciftci, F. Padinger, T. Fromherz, J. C. Hummelen, *Appl. Phys. Lett.* **2001**, *78*, 841.
[6] P. Peumans, A. Yakimov, S. R. Forrest, *J. Appl. Phys.* **2003**, *93*, 3693.
[7] W. Ma, C. Yang, X. Gong, K. Lee, A. J. Heeger, *Adv. Funct. Mater.* **2005**, *15*, 1617.
[8] Y. Liang, Z. Xu, J. Xia, S.-T. Tsai, Y. Wu, G. Li, C. Ray, L. Yu, *Adv. Mater.* **2010**, E135.
[9] M. Riede, C. Uhrich, J. Widmer, R. Timmreck, D. Wynands, G. Schwartz, W.-M. Gnehr, D. Hildebrandt, A. Weiss, J. Hwang, S. Sudharka, P. Erk, M. Pfeiffer, K. Leo, *Adv. Funct. Mater.* **2011**, *21*, 3019.
[10] Y. S. Chen, X. J. Wan, G. K. Long, *Acc. Chem. Res.* **2013**, *46*, 2645.
[11] M. Berggren, O. Inganäs, G. Gustafsson, J. Rasmusson, M. R. Andersson, T. Hjertberg, O. Wennerstrom, *Nature* **1994**, *372*, 444.
[12] S. R. Forrest, *Org. Electron.* **2003**, *4*, 45.
[13] S. Reineke, M. Thomschke, B. Lüssem, K. Leo, *Rev. Mod. Phys.* **2013**, *85*, 1245.
[14] K. Walzer, B. Maennig, M. Pfeiffer, K. Leo, *Chem. Rev.* **2007**, *107*, 1233.
[15] A. R. Brown, A. Pomp, C. M. Hart, D. M. de Leeuw, *Science* **1995**, *270*, 972.
[16] A. Dodabalapur, L. Torsi, H. E. Katz, *Science* **1995**, *268*, 270.
[17] H. Sirringhaus, N. Tessler, R. H. Friend, *Science* **1998**, *280*, 1741.
[18] G. Horowitz, *Adv. Mater.* **1998**, *10*, 365.
[19] M. E. Gershenson, V. Podzorov, A. F. Morpurgo, *Rev. Mod. Phys.* **2006**, *78*, 973.

[20] Plastic Logic Ltd, Plastic Logic Unveils Latest Fully Flexible All Plastic AMOLED Display, http://www.plusplasticelectronics.com/ (accessed: July **2014**).
[21] K. Myny, E. van Veenendaal, G. H. Gelinck, J. Genoe, W. Dehaene, P. Heremans, *IEEE J. Solid State Circ.* **2012**, *47*, 284.
[22] F. Alibart, S. Pleutin, O. Bichler, C. Gamrat, T. Serrano-Gotarredona, B. Linares-Barranco, D. Vuillaume, *Adv. Func. Mater.* **2012**, *22*, 609.
[23] G. Gelinck, P. Heremans, K. Nomoto, T. D. Anthopoulos, *Adv. Mater.* **2010**, *22*, 3778.
[24] M. L. Hammock, A. Chortos, B. C. K. Tee, J. B. H. Tok, Z. Bao, *Adv. Mater.* **2013**, *25*, 5997.
[25] K. Tybrandt, R. Forchheimer, M. Berggren, *Nat. Commun.* **2012**, *3*, 871.
[26] M. D. Angione, R. Pilolli, S. Cotrone, M. Magliulo, A. Mallardi, G. Palazzo, L. Sabbatini, D. Fine, A. Dodabalapur, N. Cioffi, L. Torsi, *Mater. Today* **2011**, *14*, 424.
[27] J. S. Brooks, D. L. Eaton, J. E. Anthony, S. R. Parkin, J. W. Brill, Y. Sushko, *Curr. Appl. Phys.* **2001**, *1*, 301.
[28] J. E. Anthony, J. S. Brooks, D. L. Eaton, S. R. Parkin, *J. Am. Chem. Soc.* **2001**, *123*, 9482.
[29] Y.-Y. Lin, D. J. Gundlach, S. F. Nelson, T. N. Jackson, *IEEE Electr. Dev. Lett.* **1997**, *18*, 606.
[30] H. Klauk, M. Halik, U. Zschieschang, G. Schmid, W. Radlik, W. Weber, *Appl. Phys. Lett.* **2002**, *92*, 5259.
[31] S. K. Park, T. N. Jackson, J. E. Anthony, D. A. Mourey, *Appl. Phys. Lett.* **2007**, *91*, 063514.
[32] J.-F. Chang, T. Sakanoue, Y. Olivier, T. Uemura, M.-B. Dufourg-Madec, S. G. Yeates, J. Cornil, J. Takeya, A. Troisi, H. Sirringhaus, *Phys. Rev. Lett.* **2011**, *107*, 066601.
[33] B. D. Naab, S. Himmelberger, Y. Diao, K. Vandewal, P. Wei, B. Lüssem, A. Salleo, Z. Bao, *Adv. Mater.* **2013**, *25*, 4663.
[34] J. A. Lim, W. H. Lee, H. S. Lee, J. H. Lee, Y. D. Park, K. Cho, *Adv. Mater.* **2008**, *18*, 229.
[35] H. Sirringhaus, *Adv. Mater.* **2005**, *17*, 2411.
[36] V. Coropceanu, J. Cornil, D. A. da Silva Filho, Y. Olivier, R. Silbey, J.-L. Brédas, *Chem. Rev.* **2007**, *107*, 926.
[37] M. Mas-Torrent, C. Rovira*Chem. Rev.* **2011**, *111*, 4833.
[38] Y. Olivier, D. Niedzialek, V. Lemaur, W. Pisula, K. Müllen, U. Koldemir, J. R. Reynolds, R. Lazzaroni, J. Cornil, D. Beljonne, *Adv. Mater.* **2014**, *26*, 2119.
[39] *Introducing Molecular Electronics*, (Eds: G. Cuniberti, G. Fagas, K. Richter), Springer-Verlag, Berlin, Germany **2005**.
[40] J. C. Cuevas, E. Scheer, *Molecular Electronics*, World Scientific, Singapore **2010**.
[41] J. Park, A. N. Pasupathy, J. I. Goldsmith, C. Chang, Y. Yaish, J. R. Petta, M. Rinkoski, J. P. Sethna, H. D. Abruna, P. L. McEuen, D. C. Ralph, *Nature* **2002**, *417*, 722.
[42] W. Liang, M. P. Shores, M. Bockrath, J. R. Long, H. Park, *Nature* **2002**, *417*, 725.
[43] X. D. Cui, A. Primak, X. Zarate, J. Tomfohr, O. F. Sankey, A. L. Moore, T. A. Moore, D. Gust, G. Harris, S. M. Lindsay, *Science* **2001**, *294*, 571.
[44] A. Aviram, M. A. Ratner, *Chem. Phys. Lett.* **1974**, *29*, 277.
[45] G. J. Ashwell, J. R. Sambles, A. S. Martin, W. G. Parkerb, M. Szablewski, *J. Chem. Soc., Chem. Commun.* **1990**, 1374.
[46] R. M. Metzger, B. Chen, U. Hopfner, M. V. Lakshmikantham, D. Vuillaume, T. Kawai, X. Wu, H. Tachibana, T. V. Hughes, H. Sakurai, J. W. Baldwin, C. Hosch, M. P. Cava, L. Brehmer, G. J. Ashwell, *J. Am. Chem. Soc.* **1997**, *119*, 10455.
[47] L. Zhu, Y. Yi, Y. Li, E.-G. Kim, V. Coropceanu, J.-L. Brédas, *J. Am. Chem. Soc.* **2012**, *134*, 2340.
[48] S. Datta*Electronic Transport in Mesoscopic Systems*, Cambridge University Press, UK **1999**.
[49] H. Park, J. Park, A. K. L. Lim, E. H. Anderson, A. P. Alivisatos, P. L. McEuen, *Nature* **2000**, *407*, 57.
[50] H. Kleemann, R. Gutierrez, F. Lindner, S. Avdoshenko, P. D. Manrique, B. Lüssem, G. Cuniberti, K. Leo, *Nano Lett.* **2010**, *10*, 4929.
[51] J. D. Scott, L. D. Bozano, *Adv. Mater.* **2007**, *19*, 1452.
[52] K. Blum, *Density Matrix Theory and Applications*, Plenum Press, New York, USA **1981**.
[53] H. Klauk, *Chem. Soc. Rev.* **2010**, *39*, 2643.
[54] Y. Yuan, G. Giri, A. Ayzner, A. Zoombelt, S. Mannsfeld, J. Chen, D. Nordlund, M. F. Toney, J. Huang, Z. Bao, *Nat. Commun.* **2014**, *5*, 3005.
[55] H. Okamoto, S. Hamao, H. Goto, Y. Sakai, M. Izumi, S. Gohda, Y. Kubozono, R. Eguchi, *Sci. Rep.* **2014**, *4*, 5048.
[56] I. N. Hulea, S. Fratini, H. Xie, C. L. Mulder, N. N. Iossad, G. Rastelli, S. Ciuchi, A. F. Morpurgo, *Nat. Mater.* **2006**, *5*, 982.
[57] V. Podzorov, E. Menard, A. Borissov, V. Kiryukhin, J. A. Rogers, M. E. Gershenson, *Phys. Rev. Lett.* **2004**, *93*, 086602.
[58] A. S. Molinari, H. Alves, Z. Chen, A. Facchetti, A. F. Morpurgo, *J. Am. Chem. Soc.* **2009**, *131*, 2462.
[59] J. Soeda, T. Uemura, Y. Mizuno, A. Nakao, Y. Nakazawa, A. Facchetti, J. Takeya, *Adv. Mater.* **2011**, *23*, 3681.
[60] V. C. Sundar, J. Zaumseil, V. Podzorov, E. Menard, R. L. Willet, T. Someya, M. E. Gershenson, J. A. Rogers, *Science* **2004**, *303*, 1644.
[61] I. Lezama, A. Morpurgo, *MRS Bull.* **2013**, *38*, 51.
[62] R. H. M. Smit, Y. Noat, C. Untied, N. D. Lang, M. C. van Hemert, J. M. van Ruitenbeek, *Nature* **2002**, *419*, 906.
[63] M. Kiguchi, O. Tal, S. Wohlthat, F. Pauly, M. Krieger, D. Djukic, J. C. Cuevas, J. M. van Ruitenbeek, *Phys. Rev. Lett.* **2008**, *101*, 046801.
[64] C. Joachim, J. K. Gimzewski, R. R. Schlitter, C. Chavy, *Phys. Rev. Lett.* **1995**, *74*, 2102.
[65] M. A. Reed, C. Zhou, C. J. Muller,T. P. Burgin , J. M. Tour, *Science* **1997**, *278*, 252.
[66] J. Reichert, R. Ochs, D. Beckmann, H. B. Weber, M. Mayor, H. v. Löhneysen, *Phys. Rev. Lett.* **2002**, *88*, 176804.
[67] E. Lörtscher, *Nat. Nanotechnol.* **2013**, *8*, 381.
[68] S. Kubatkin, A. Danilov, M. Hjort, J. Cornil, J.-L. Brédas, N. Stuhr-Hansen, P. Hedegård, T. Bjørnholm, *Nature* **2003**, *425*, 698.
[69] H. Song, Y. Kim, Y. H. Jang, H. Jeong, M. A. Reed, T. Lee, *Nature* **2009**, *462*, 1039.
[70] R. Landauer, *IBM J. Res. Dev.* **1988**, *32*, 306.
[71] R. Landauer, *Phys. Scr.* **1992**, *T42*, 110.
[72] J. Maassen, F. Zahid, H. Guo, *Phys. Rev. B* **2009**, *80*, 125423.
[73] M. Dey, S. K. Maiti, S. N. Karmakar, *Org. Electron.* **2011**, *12*, 2017.
[74] C. J. Cattena, R. A. Bustos-Marun, H. M. Pastawski, *Phys. Rev. B* **2010**, *82*, 144201.
[75] D. Nozaki, C. Gomes da Rocha, H. M. Pastawski, G. Cuniberti, *Phys. Rev. B* **2012**, *85*, 155327.
[76] S. H. Choi, B. Kim, C. D. Frisbie, *Science* **2008**, *320*, 1482.
[77] W. B. Davis, W. A. Svec, M. A. Ratner, M. R. Wasielewski, *Nature* **1998**, *396*, 60.
[78] B. Giese, J. Amaudrut, A. K. Kohler, M. Spormann, S. Wessely, *Nature* **2001**, *412*, 318.
[79] J. L. D'Amato, H. M. Pastawski, *Phys. Rev. B* **1990**, *41*, 7411.
[80] a)M. Büttiker, *Phys. Rev. B* **1985**, *32*, 1846(R); *IBM J. Res. Dev.* **1988**, *32*, 63.
[81] H. M. Pastawski, L. E. F. Foa Torres, E. Medina, *Chem. Phys.* **2002**, *281*, 257.
[82] F. Ortmann, F. Bechstedt, K. Hannewald, *Phys. Stat. Sol.* **2011**, *248*, 511.
[83] T. Holstein, *Ann. Phys.* **1959**, *8*, 325.
[84] T. Holstein, *Ann. Phys.* **1959**, *8*, 343.

[85] K. S. Radke, R. Scholz, F. Ortmann, K. Leo, G. Cuniberti, *J. Phys. Chem. C* **2014**, *118*, 6537.
[86] Z. J. Donhauser, B. A. Mantooth, K. F. Kelly, L. A. Bumm, J. D. Monnell, J. J. Stapleton, D. W. PriceJr., A. M. Rawlett, D. L. Allara, J. M. Tour, P. S. Weiss, *Science* **2001**, *292*, 2303.
[87] L. Venkataraman, J. E. Klare, C. Nuckolls, M. S. Hybertsen, M. L. Steigerwald, *Nature* **2006**, *442*, 904.
[88] S. Stöttinger, G. Hinze, G. Diezemann, I. Oesterling, K. Müllen, T. Basché, *Nat. Nanotechnol.* **2014**, *9*, 182.
[89] C. P. Collier, G. Mattersteig, E. W. Wong, Y. Luo, K. Beverly, J. Sampaio, F. M. Raymo, J. Fraser Stoddart, J. R. Heath, *Science* **2000**, *289*, 1172.
[90] J.-L. Brédas, D. Beljonne, V. Coropceanu, J. Cornil, *Chem. Rev.* **2004**, *104*, 4971.
[91] R. C. Jaklevic, J. Lambe, *Phys. Rev. Lett.* **1966**, *17*, 1139.
[92] M. Galperin, M. A. Ratner, A. Nitzan, *J. Phys. Condens. Matter* **2007**, *19*, 103201.
[93] J. Kirtley, D. J. Scalapino, P. K. Hansma, *Phys. Rev. B* **1976**, *14*, 3177.
[94] J. Kirtley, J. T. Hall, *Phys. Rev. B* **1980**, *22*, 848.
[95] M. Galperin, M. A. Ratner, A. Nitzan, *J. Chem. Phys.* **2004**, *121*, 11965.
[96] B. C. Stipe, M. A. Rezaei, W. Ho, *Science* **1998**, *280*, 1732.
[97] W. Wang, T. Lee, I. Kretzschmar, M. A. Reed, *Nano Lett.* **2004**, *4*, 643.
[98] J. G. Kushmerick, J. Lazorcik, C. H. Patterson, R. Shashidhar, *Nano Lett.* **2004**, *4*, 639.
[99] H. Song, Y. Kim, J. Ku, Y. H. Jang, H. Jeong, T. Lee, *Appl. Phys. Lett.* **2009**, *94*, 103110.
[100] A. N. Pasupathy, J. Park, C. Chang, A. V. Soldatov, S. Lebedkin, R. C. Bialczak, J. E. Grose, L. A. K. Donev, J. P. Sethna, D. C. Ralph, P. L. McEuen, *Nano Lett.* **2005**, *5*, 203.
[101] S. Gélinas, A. Rao, A. Kumar, S. L. Smith, A. W. Chin, J. Clark, T. S. van der Poll, G. C. Bazan, and RichardH. Friend, *Science* **2014**, *343*, 512.
[102] K. Hannewald, V. M. Stojanovic, J. M. T. Schellekens, P. A. Bobbert, G. Kresse, J. Hafner, *Phys. Rev. B* **2004**, *69*, 075211.
[103] D. A. da Silva Filho, E. G. Kim, J. L. Brédas, *Adv. Mater.* **2005**, *17*, 1072.
[104] F. Ortmann, K. Hannewald, F. Bechstedt, *Phys. Rev. B* **2007**, *75*, 195219.
[105] F. Ortmann, K. Hannewald, F. Bechstedt, *J. Phys. Chem. B* **2008**, *112*, 1540.
[106] V. Stehr, J. Pfister, R. F. Fink, B. Engels, C. Deibel, *Phys. Rev. B* **2011**, *83*, 155208.
[107] H. Oberhofer, J. Blumberger, *Phys. Chem. Chem. Phys.* **2012**, *14*, 13846.
[108] A. Girlando, M. Masino, I. Bilotti, A. Brillante, R. G. Della Valle, E. Venuti, *Phys. Chem. Chem. Phys.* **2012**, *14*, 1694.
[109] C. Sutton, J. S. Sears, V. Coropceanu, J.-L. Brédas, *J. Phys. Chem. Lett.* **2013**, *4*, 919.
[110] H. Ishii, N. Kobayashi, K. Hirose, *Phys. Rev. B* **2013**, *88*, 205208.
[111] S. Hasegawa, T. Mori, K. Imaeda, S. Tanaka, Y. Yamashita, H. Inokuchi, H. Fujimoto, K. Seki, N. Ueno*J. Chem. Phys.* **1994**, *100*, 6969.
[112] N. Koch, A. Vollmer, I. Salzmann, B. Nickel, H. Weiss, J. P. Rabe, *Phys. Rev. Lett.* **2006**, *96*, 156803.
[113] G. Koller, S. Berkebile, M. Oehzelt, P. Puschnig, C. Ambrosch-Draxl, F. P. Netzer, M. G. Ramsey, *Science* **2007**, *317*, 351.
[114] S. Machida, Y. Nakayama, S. Duhm, Q. Xin, A. Funakoshi, N. Ogawa, S. Kera, N. Ueno, H. Ishii, *Phys. Rev. Lett.* **2010**, *104*, 156401.
[115] R. C. Hatch, D. L. Huber, H. Höchst, *Phys. Rev. Lett.* **2010**, *104*, 047601.
[116] F. Bussolotti, Y. Yamada-Takamura, Y. Wang, R. Friedlein, *J. Chem. Phys.* **2011**, *135*, 124709.
[117] S. Ciuchi, R. C. Hatch, H. Höchst, C. Faber, X. Blase, S. Fratini, *Phys. Rev. Lett.* **2012**, *108*, 256401.
[118] M. Wießner, J. Ziroff, F. Forster, M. Arita, K. Shimada, P. Puschnig, A. Schöll, F. Reinert, *Nat. Comm.* **2013**, *4*, 1514.
[119] N. Karl, in *Landolt-Börnstein Numerical data and functional relationships in science and technology (New Series), Vol 17i, Group III*, (Eds: O. Madelung, M. Schulz, and H. Weiss), Springer-Verlag, Berlin, Germany **1985**, p 106.
[120] C. Reese, Z. Bhao, *Mater. Today* **2007**, *10*, 27.
[121] F. Ortmann, K. Hannewald, F. Bechstedt, *J. Phys. Chem. B* **2009**, *113*, 7367.
[122] B. Bräuer, A. Virkar, S. C. B. Mannsfeld, D. P. Bernstein, R Kukreja, K. W. Chou, T. Tyliszczak, Z. Bao, Y. Acremann, *Chem. Mater.* **2010**, *22*, 3693.
[123] H. Yamane, N. Kosugi, *Phys. Rev. Lett.* **2013**, *111*, 086602.
[124] A. Troisi, G. Orlandi, *J. Phys. Chem. A* **2006**, *110*, 4065.
[125] K. Hannewald, P. A. Bobbert, *Phys. Rev. B* **2004**, *69*, 075212.
[126] W. Warta, N. Karl, *Phys. Rev. B* **1985**, *32*, 1172.
[127] K. Hannewald, P. A. Bobbert, *Appl. Phys. Lett.* **2004**, *85*, 1535.
[128] R. A. Marcus, *J. Chem. Phys.* **1956**, *24*, 966.
[129] V. G. Levich, *Adv. Electrochem. Electrochem. Eng.* **1966**, *4*, 249.
[130] J. Jortner, *J. Chem. Phys.* **1976**, *64*, 4860.
[131] R. Kubo, *J. Phys. Soc. Jap.* **1957**, *12*, 570.
[132] F. Ortmann, F. Bechstedt, K. Hannewald, *Phys. Rev. B* **2009**, *79*, 235206.
[133] J. M. Ziman, *Electrons and Phonons*, Clarendon Press, Oxford, UK **2007**.
[134] F. Ortmann, S. Roche, *Phys. Rev. B* **2011**, *84*, 180302(R).
[135] A. Troisi, G. Orlandi, *Phys. Rev. Lett.* **2006**, *96*, 086601.
[136] S. Ciuchi, S. Fratini, D. Mayou, *Phys. Rev. B* **2011**, *83*, 081202(R).
[137] a)H. Ishii, K. Honma, N. Kobayashi, Kenji Hirose, *Phys. Rev. B* **2012**, *285*, 245206; b)H. Tamura, M. Tsukada, H. Ishii, N. Kobayashi, K. Hirose, *ibid.* **2012**, *86*, 035208.
[138] C. Gollub, S. Avdoshenko, R. Gutierrez, Y. Berlin, G. Cuniberti, *Isr. J. Chem.* **2012**, *52*, 452.
[139] H. Bässler, *Phys. Stat. Sol. B* **1993**, *175*, 15.
[140] A. Miller, E. Abrahams, *Phys. Rev.* **1960**, *120*, 745.
[141] M. Brandbyge, J.-L. Mozos, P. Ordejón, J. Taylor, K. Stokbro, *Phys. Rev. B.* **2002**, *65*, 165401.
[142] Y. Xue, M. A. Ratner, *Phys. Rev. B* **2003**, *68*, 115406.
[143] G. Heimel, S. Duhm, I. Salzmann, A. Gerlach, A. Strozecka, J. Niederhausen, C. Bürker, T. Hosokai, I. Fernandez-Torrente, G. Schulze, S. Winkler, A. Wilke, R. Schlesinger, J. Frisch, B. Bröker, A. Vollmer, B. Detlefs, J. Pflaum, S. Kera, K. J. Franke, N. Ueno, J. I. Pascual, F. Schreiber, N. Koch, *Nature Chem.* **2013**, *5*, 187.
[144] R. M. Dreizler, E. K. U. Gross, *Density Functional Theory*, Springer Verlag, Berlin, Germany **1990**.
[145] W. Kohn, L. J. Sham, *Phys. Rev.* **1965**, *140*, A1133.
[146] J. P. Perdew, *Phys. Rev. Lett.* **1985**, *55*, 1665.
[147] S. Grimme, *J. Comput. Chem.* **2004**, *25*, 1463.
[148] F. Ortmann, F. Bechstedt, W. G. Schmidt, *Phys. Rev. B* **2006**, *73*, 205101.
[149] A. Tkatchenko, M. Scheffler, *Phys. Rev. Lett.* **2009**, *102*, 073005.
[150] A. D. Becke, *J. Chem. Phys.* **1993**, *98*, 1372.
[151] C. Faber, J. Laflamme Janssen, M. Côté, E. Runge, X. Blase, *Phys. Rev. B* **2011**, *84*, 155104.
[152] P. Löwdin, *J. Chem. Phys.* **1950**, *18*, 365.
[153] K. Kudo, M. Yamashina, T. Moriizumi, *Jpn. J. Appl. Phys.* **1984**, *23*, 130.
[154] A. Tsumura, H. Koezuka, T. Ando, *Appl. Phys. Lett.* **1986**, *49*, 1210.
[155] H. Koezuka, A. Tsumura, T. Ando, *Synth. Met.* **1987**, *18*, 699.

[156] A. Hoppe, D. Knipp, B. Gburek, A. Benor, M. Marinkovic, V. Wagner, *Org. Electron.* **2010**, *11*, 626.
[157] A. Fischer, R. Scholz, K. Leo, B. Lüssem, *Appl. Phys. Lett.* **2012**, *101*, 213303.
[158] J. Zaumseil, H. Sirringhaus, *Chem. Rev.* **2007**, *107*, 1296.
[159] J. E. Anthony, A. Facchetti, M. Heeney, S. R. Marder, Xiaowei Zhan, *Adv. Mater.* **2010**, *22*, 3876.
[160] D. M. deLeeuw, M. M. J. Simenon, A. R. Brown, R. E. F. Einerhand, *Synth. Met.* **1997**, *87*, 53.
[161] Z. A. Bao, A. J. Lovinger, J. Brown, *J. Am. Chem. Soc.* **1998**, *120*, 207.
[162] B. A. Jones, M. J. Ahrens, M. H. Yoon, A. Facchetti, T. J. Marks, M. R. Wasielewski, *Angew. Chem. Int. Ed.* **2004**, *43*, 6363.
[163] M. Stolte, S. L. Suraru, F. Würthner, J. H. Oh, Z. Bao, J. Brill, M. Könemann, J. Qu, U. Zschieschang, H. Klauk, *Proc. SPIE* **2010**, *7778*, 777804.
[164] R. Rödel, F. Letzkus, T. Zaki, J. N. Burghartz, U. Kraft, U. Zschieschang, K. Kern, H. Klauk, *Appl. Phys. Lett.* **2013**, *102*, 233303.
[165] L.-L. Chua, J. Zaumseil, J.-F. Chang, E.C.-W. Ou, P.K.-H. Ho, H. Sirringhaus, R. H. Friend, *Nature* **2005**, *434*, 194.
[166] N. Benson, M. Schidleja, C. Melzer, R. Schmechel, H. von Seggern, *Appl. Phys. Lett.* **2006**, *89*, 182105.
[167] J. Collet, O. Tharaud, A. Chapoton, D. Vuillaume, *Appl. Phys. Lett.* **2000**, *76*, 1941.
[168] F. Ante, D. Kälblein, T. Zaki, U. Zschieschang, T. Canzler, A. Werner, K. Takimiya, M. Ikeda, T. Sekitani, T. Someya, H. Klauk, *Small* **2011**, *7*, 1186.
[169] G. Horowitz, *Adv. Poly. Sci.* **2010**, *223*, 113.
[170] P. Bobbert, A. Sharma, S. Mathijssen, M. Kemerink, D. M. de Leeuw, *Adv. Mater.* **2012**, *24*, 1146.
[171] J. Haddock, X. Zhang, S. Zheng, Q. Zhang, S. Marder, B. Kippelen, *Org. Elec.* **2006**, *7*, 45.
[172] L. Torsi, A. Dodabalapur, H. E. Katz, *J. Appl. Phys.* **1995**, *78*, 1088.
[173] H. Klauk, G. Schmid, W. Radlik, W. Weber, L. Zhou, C. Sheraw, J. Nichols, T. Jackson, *Solid State Electron.* **2003**, *47*, 293.
[174] S. Locci, M. Morana, E. Orgiu, A. Bonfiglio, P. Lugli, *IEEE Transact. Elec. Dev.* **2008**, *55*, 2561.
[175] S. Wang, Y. Yan, K. Tsukagoshi, *Appl. Phys. Lett.* **2010**, *97*, 063307.
[176] Y. Xu, C. Liu, H. Sun, F. Balestra, G. Ghibaudo, W. Scheideler, Y. Noh, *Org. Electron.* **2014**, in press.
[177] S. Wang, T. Minari, T. Miyadera, K. Tsukagoshi, Y. Aoyagi, *Appl. Phys. Lett.* **2007**, *91*, 203508.
[178] D. Khim, K. Baeg, J. Kim, J. Yeo, M. Kang, P. S. K. Amegadzea, M. Kim, J. Cho, J. H. Lee, D. Kim, Y. Noh, *J. Mater. Chem.* **2012**, *22*, 16979.
[179] S. Hoshino, S. Nagamatsu, M. Chikamatsu, M. Misaki, Y. Yoshida, N. Tanigaki, K. Yase, *Synth. Met.* **2003**, *137*, 953.
[180] Z. Wang, M. Waqas Alam, Y. Lou, S. Naka, H. Okada, *Appl. Phys. Lett.* **2012**, *100*, 043302.
[181] T. Matsumoto, W. Ou-Yang, K. Miyake, T. Uemura, J. Takeya, *Org. Elec.* **2013**, *14*, 2590.
[182] S. Nicht, H. Kleemann, A. Fischer, K. Leo, B. Lüssem, *Org. Elec.* **2014**, *15*, 654.
[183] S. Singh, S. Mohapatra, A. Sharma, C. Fuentes-Hernandez, S. Barlow, S. Marder, B. Kippelen, *Appl. Phys. Lett.* **2013**, *102*, 153303.
[184] T. N. Ng, J. A. Marohn, M. L. Chabinyc, *J. Appl. Phys.* **2006**, *100*, 084505.
[185] M. Egginger, S. Bauer, R. Schwödiauer, H. Neugebauer, N. S. Sariciftci, *Chem. Month.* **2009**, *140*, 735.
[186] S. Schiefer, M. Huth, A. Dobrinevski, B. Nickel, *J. Am. Chem. Soc.* **2007**, *129*, 10316.
[187] C. Celle, C. Suspène, M. Ternisien, S. Lenfant, D. Guérin, K. Smaali, K. Lmimouni, J. P. Simonato, D. Vuillaume, *Org. Electron.* **2014**, *15*, 729.
[188] A. Troisi, G. Orlandi, *J. Phys. Chem. B* **2005**, *109*, 1849.
[189] P. Cosseddu, G. Tiddia, S. Milita, A. Bonfiglio, *Org. Electron.* **2013**, *14*, 206.
[190] B. Lüssem, H. Kleemann, D. Kasemann, F. Ventsch, K. Leo, *Adv. Func. Mater.* **2014**, *24*, 1011.
[191] B. Lüssem, M. Tietze, H. Kleemann, C. Hoßbach, J. Bartha, A. Zakhidov, K. Leo, *Nat. Commun.* **2013**, *4*, 2775.
[192] L. Ma, Y. Yang, *App. Phys. Lett.* **2004**, *85*, 5084.
[193] M. McCarthy, B. Liu, E. P. Donoghue, I. Kravchenko, D. Y. Kim, F. So, A. G. Rinzler, *Science* **2011**, *332*, 570.
[194] A. J. Ben-Sasson, E. Avon, E. Ploshnik, O. Globerman, R. Shenhar, G. L. Frey, N. Tesler, *Appl. Phys. Lett.* **2009**, *95*, 213301.
[195] K. Nakamura, T. Hata, A. Yoshizawa, K. Obata, H. Endo, K. Kudo, *Appl. Phys. Lett.* **2006**, *89*, 103525.
[196] H. Kleemann, A. Günther, K. Leo, B. Lüssem, *Small* **2013**, *9*, 3670.
[197] M. Galperin, M. A. Ratner, A. Nitzan, *Nano Lett.* **2005**, *5*, 125.
[198] C. Westermeier, A. Cernescu, S. Amarie, C. Liewald, F. Keilmann, B. Nickel, *Nat. Commun.* **2014**, *5*, 4101.
[199] K. Asadi, A. J. Kronemeijer, T. Cramer, L. J. A. Koster, P. W. M. Blom, D. M. de Leeuw, *Nat. Commun.* **2013**, *4*, 1710.
[200] H. Geng, Q. Peng, L. Wang, H. Li, Y. Liao, Z. Ma, Z. Shuai, *Adv. Mater.* **2012**, *24*, 3568.
[201] A. P. Scott, L. Radom, *J. Phys. Chem.* **1996**, *100*, 16502.